Experimental investigation of the effects of upstream perturbations in the near-wall and core of a high porosity random-wire porous medium

A THESIS

SUBMITTED TO THE FACULTY OF THE GRADUATE SCHOOL

OF THE UNIVERSITY OF MINNESOTA

BY

Krithiga Ganesan

IN PARTIAL FULFILLMENT OF THE REQUIREMENTS

FOR THE DEGREE OF

Master of Science

October, 2010

Abstract

Experiments were conducted on a high-porosity porous medium to investigate the influences of upstream perturbations. The porous medium was fabricated by stacking stainless steel wire-mesh screens in a container of circular cross-section. A step change in porosity is considered a perturbation to the flow as these perturbations would offer an alternate path for flow. In the present set of experiments, perturbations were offered by gaps or blockages to the flow, which would allow jets or wakes to evolve inside the porous medium, , with the gap offering a low-resistance path and the blockage offering a high-resistance path. These perturbations were positioned at two radial locations: a near-wall case, with a gap or blockage adjacent to walls of the test-section container, and a core-flow case, with a hole or a blockage at the center of the metal screens. In each case, the perturbation was for half the streamwise distance of the test-section. For the remainder of the streamwise distance, flow was allowed to travel unperturbed through the porous medium. Hotwire measurements of velocity were taken at the exit of the test-section, which provided insight on the redistribution of flow for the two perturbation studies, and consequently on the characterisitics of transport in different regions of the porous medium. It was discovered that pore-scale eddies, shed from the metal wires that constitute the porous medium were suppressed near the walls of the container by the wall boundary layer, leading to very poor transport in the near-wall region. As a result, effects of the perturbations were felt even after twenty hydraulic diameters of streamwise travel. No such effects were observed when the core-flow was perturbed. These results indicated that

transport charactersitics are vastly different in different regions of the flow and near-wall transport in porous media flows is far less effective than core transport.

Contents

Abstract **i**

List of Tables **vi**

List of Figures **vii**

1 Introduction **1**

1.1 Motivation 1

1.2 Porous media flows: fundamental aspects 2

1.3 Experiments on porous media flows 10

1.4 Previous work on porous media flows with perturbations 12

1.4.1 Transport enhancement by pore-scale eddies 12

1.4.2 Upstream half-axial gap 13

1.4.3 Jet penetration through a porous medium 15

1.4.4 Near-wall transport 18

1.5 Summary of previous work 23

1.6 Scope of the present study 24

2 Experimental methods **25**

2.1 Overview 25

2.2 Methodology 26
2.3 Description of the experimental cases 28
2.3.1 Unperturbed flow (no upstream gaps or blockages) 28
2.3.2 Upstream near-wall perturbations 30
2.3.3 Upstream core-flow perturbations 31
2.4 Description of the flow facility 35
2.5 Experimental techniques 36
2.5.1 Hotwire anemometry 36
2.5.2 Instrumentation and signal conditioning 37
2.5.3 Hotwire calibration 39
2.5.4 Estimation of uncertainty 42
2.6 Qualification of measurements: Unperturbed flow experiments . . 47

3 Results: Near-wall flow perturbation experiments 52
3.1 Objectives 52
3.2 Velocity profiles 54
3.3 Integrated velocity profiles 57
3.4 Summary of near-wall perturbation experiments 60

4 Results: Core-flow perturbation experiments 73
4.1 Objectives 73
4.2 Jet spreading through the core of the porous medium 74
4.3 Wake spreading through the core of the porous medium 76

5 Pore-scale eddy transport in porous media 84

6 Conclusion and Future Work 92
6.1 Summary of results 92

6.2 Limitations of the present study and future work 93

References **95**

Appendix A. TSI 1051 Hotwire Anemometer: Operational Caveats **98**

A.1 Description of the TSI 1051 Bridge controls 98

A.2 Calibration procedure 102

Appendix B. A note on formatting using LaTeX **106**

List of Tables

2.1 Test conditions for unperturbed flow 30

2.2 Test conditions for experiments involving perturbations 34

2.3 Comparison of flow-rates to qualify measurements 48

3.1 Integrated velocity profiles with upstream blockages 58

3.2 Integrated velocity profiles with upstream gaps 58

3.3 Difference in integrated velocity profiles between unperturbed and perturbed flows 59

A.1 Normal position of the bridge controls for adjusting resistance . . 99

A.2 Normal position of the bridge controls for adjusting resistance . . 100

List of Figures

1.1 Flow visualization experiments performed by Taneda to study flow over a sphere at different Reynolds numbers. 4
1.2 Representative Elementary Volume inclusive of a few pores. 5
1.3 Jet penetration in high porosity porous media under oscillatory flow conditions. 16
1.4 Near-wall channeling of flow and variable porosity. 19
2.1 A schematic of the near-wall perturbation experiments 32
2.2 A schematic of the core-flow perturbation experiments 33
2.3 A schematic of the test-facility 36
2.4 Schematic of a constant temperature anemometer 39
2.5 TSI 1211-T1.5 sensor and its dimensions 40
2.6 Schematic of the instrumentation used for data-acquisition 41
2.7 A schematic of the calibration rig 43
2.8 Calibration data with polynomial fit 44
2.9 Goodness of the curve-fits 45
2.10 Goodness of the polynomial fit 46
2.11 Exit-plane velocity profiles for unperturbed flow 50
2.12 Exit-plane velocity profiles for unperturbed flow 51
3.1 Near-wall flow measurement locations 53

3.2 Velocity profiles with upstream blockage 62
3.3 Near-wall velocity profiles with upstream blockage 63
3.4 Velocity profiles with upstream gap 64
3.5 Near-wall profiles with upstream gap 65
3.6 Circumferential variation of velocity profiles 66
3.7 Circumferential variation of velocity profiles 67
3.8 Circumferential variation of velocity profiles 68
3.9 Near-wall velocity profile with and without a gap 69
3.10 Near-wall velocity profile with and without a gap 70
3.11 Near-wall velocity profile with and without a blockage 71
3.12 Near-wall velocity profile with and without a blockage 72
4.1 Upstream disturbances to core-flow 74
4.2 Velocity profiles with an upstream jet in the core 79
4.3 Representative velocity profile with an upstream jet in the core . . 80
4.4 Velocity profiles with an upstream wake in the core 81
4.5 Representative velocity profile with an upstream jet in the core . . 82
4.6 Comparison of profiles with an upstream jet and a wake 83
5.1 Eddy dispersion in the near-wall region obtained by mixing-length hypothesis 90

Chapter 1

Introduction

1.1 Motivation

Engineering applications of porous media such as regenerators and baffled heat exchangers tend to involve porous media with irregular geometries sandwiched in a container. Fabrication and assembly processes create porous ducts with gaps where an annular gap opens up between the porous medium and the walls of the duct creating an alternate flow path; thermal effects such as growth or shrinkage of the medium can also create a gap or a blockage. Flow through such irregular geometries will have features that are different from flow through a "pattern" porous medium with distributed pores that are often encountered in many numerical and experimental studies.

A gap creates a low-resistance path for flow, resulting in fluid rushing to the gap; a blockage, on the contrary, results in migration of fluid away from the

blockage. Presence of gaps and blockages within the porous medium results in the development of jets and wakes inside the porous medium. The growth and spreading of these jets and wakes alter transport characteristics of the porous medium.

The focus of the present study is to expand fundamental understanding on porous media flows subjected to disturbances such as a gap or blockage. Features that appear and evolve inside a porous medium as a result of the presence of an upstream disturbance are of interest in the present study. The upstream disturbances of this study extend half the test section axial-length. The nature of the flow subject to upstream gaps and blockages are documented for two radial locations; one near the wall of the test-section and the other in the core of the porous matrix far away from the wall are documented.

1.2 Porous media flows: fundamental aspects

Some of the features that are intrinsic to porous media flows are of consideration in this section. Porous media are used in a variety of engineering applications, such as heat exchangers, regenerators in Stirling cycle engines for power generation and cryocooling applications, filters and catalytic converters, and in energy storage devices. Several types of porous media exist, such as ceramic and metal foams, particle beds, random-wire mesh screens etc. Understanding transport in porous media, hence, is critical to several applications. A porous medium is comprised of distributed solid obstructions placed inside a container through which fluid flows. The distributed solid obstructions offer resistance to the flow; in this sense, the porous medium behaves like small regions of distributed low and high flow

resistances zones.

The transport characteristics of the porous medium depend on the structural features of the porous medium. Flow through a porous medium with a large fraction of void volume will have features that are vastly different from those through a porous medium with a large fraction of solid volume, since large void spaces create paths of low resistance. One of the parameters that quantifies the structure of the porous medium is the porosity ϕ, defined as:

$$\phi = \frac{V_f}{V} \tag{1.1}$$

Here, V_f is the void volume and V is the total volume. Porosity, hence, is a measure of the volume available for fluid flow. At the pore level fluid particles encounter obstructions due to the presence of solids and this changes the fluid path within the pores.

To understand fluid-path in porous media, let us first consider flow over a single solid obstruction, such as a cylinder. Considering the cylinder diameter, D, and the approach flow velocity, U, as the characteristic length-scale and characteristic velocity, respectively, Reynolds number for the flow can be defined as:

$$Re = \frac{UD}{\nu} \tag{1.2}$$

When the Reynolds number is small (~ 1), inertial forces are negligible, and flow over the cylinder is represented by Stokes flow (Figure 1.1(a)). The flow is symmetric, i.e. flow features are identical on either side of the cylinder. The viscous drag (Stokes drag) scales on the approach flow velocity. For Reynolds

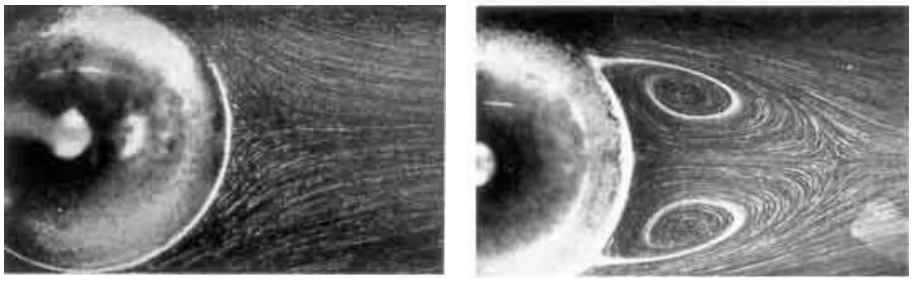

(a) Re ~ 9 (b) Re ~ 75

Figure 1.1: Flow visualization experiments to study flow over a sphere at different Reynolds numbers performed by Taneda (1956)

numbers greater than one, and typically of the order of 10 and above, boundary layer separation can be observed and eddies are shed periodically downstream of the cylinder (Figure 1.1(b)). This flow regime is characterized by these "inertial effects" and the inertial drag scales on the square of the velocity. The streamlines take a tortuous path because of the presence of the cylinder.

Flow through a porous medium is similar in many aspects to flow over a bundle of cylinders. In a sense, the porous medium behaves like an agglomeration of many cylinders. The fluid enters the porous medium and takes a tortuous path. Rather than representing this complex flow at the pore level by describing flow paths at the pore scale, the flow can be described by considering scales larger than one pore known as the "Representative Elementary Volume" (REV). Figure 1.2 shows a schematic of a REV. Doing so erases features that are local to a pore. Drawing similarties to flow over a cylinder, two features that govern transport in porous media arising from pore-scale information are the resistance offered by the solids in the porous medium (similar to the viscous and inertial drag), and transport enhancement due to eddies shed from the porous medium.

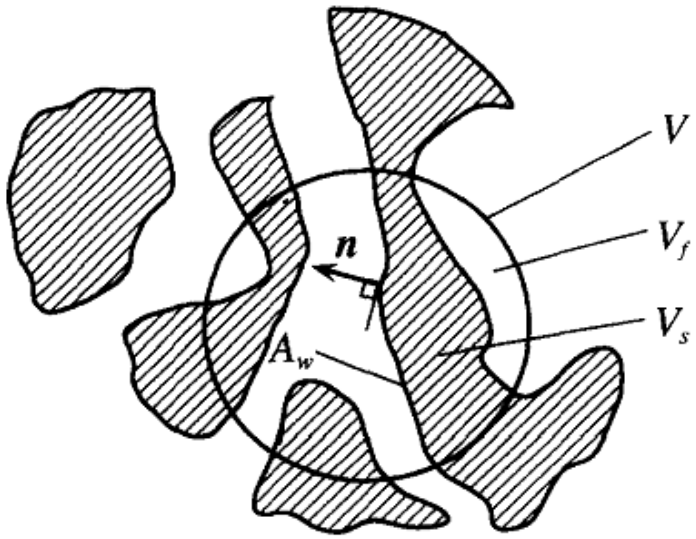

Figure 1.2: Representative Elementary Volume inclusive of a few pores. Figure adopted from Masuoka and Takatsu (1996)

Two resistances to flow which act as momentum sinks can be observed similar to the viscous and inertial drag for flow over a cylinder: (a) Viscous resistance or Darcy resistance, which is the resistance encountered by the fluid at low Reynolds numbers (similar to creeping flow over a cylinder) and (b) Inertial resistance, which is the resistance encountered due to local separation at the solid boundaries of the porous medium. This resistance occurs at moderate Reynolds numbers. An additional effect that arises due to the presence of solids which obstruct the flow is pore-scale transport enhancement due to eddies which are shed from the mean flow. This term is referred to as the "eddy dispersion".

Magnitudes of resistances and eddy dispersion can be quantified in terms of (pore) average length and velocity scales that are representative of the porous medium. As noted earlier, different types of porous media are commonly employed, such

as random-wire matrices, packed beds, metal foams, etc. The structural arrangements of pores in each of these media are different from each other. A characteristic pore-scale must be one which represents an average size of the pore, regardless of the topology of the pore and structural arrangement of solids. A common length scale employed for this purpose is the hydraulic diameter D_h, defined as:

$$D_h = \frac{\phi D_s}{1 - \phi} \tag{1.3}$$

Here, ϕ is the porosity and D_s is the diameter (or characteristic size) of the solids that constitute the porous medium. The hydraulic diameter (sometimes referred to as pore-diameter) is considered to be the characteristic length scale of the porous medium in the literature.

The characteristic velocity is the Darcy velocity, obtained by volume-averaging the local pore-velocity over several pores. It is expressed as:

$$U_D = \frac{1}{V} \int_V U dV \tag{1.4}$$

Here, U is the velocity in a pore of size dV. The volume-average operator, $\int_V$ is applied over a volume V inclusive of several pores and is larger than the volume of a single pore.

Now that the average length and velocity scales have been defined, the resistances to flow can be quantified. The resistance due to the presence of the porous medium, R, can be written as:

$$R = R_V + R_I \tag{1.5}$$

Here, R_V and R_I are the viscous and inertial resistances, respectively. The total resistance can be cast in terms of the characteristic length scale and velocity:

$$R = \frac{\mu U_D}{\sqrt{K}} + C\rho U_D^2 \tag{1.6}$$

As noted earlier, the viscous resistance, $\frac{\mu U_D}{\sqrt{K}}$, scales on the Darcy velocity, and the inertial resistance (sometimes referred to as Forchheimer resistance), $C\rho U_D^2$, scales on the square of the Darcy velocity similar to viscous and inertial drag for flow over a single cylinder.

Equation (1.6) is typically obtained by computing the flow at the pore-scale and quantifying resistances from such a computation, or experimentally determined from measured pressure drop and flow rate through the porous medium and employing empirical curve-fitting procedures.

Hsu and Cheng (1990) have derived the "macroscopic" momentum equation for a representative elementary volume of the porous medium by volume-averaging the momentum equation of a fluid element in a pore ("microscopic" momentum equation):

$$\rho_f \left[\frac{\partial \mathbf{U}}{\partial t} + \nabla . (\mathbf{U}\mathbf{U}) + \nabla . \left(\overline{\tilde{\mathbf{U}}\tilde{\mathbf{U}}} \right) \right] = -\nabla p + \mu_f \nabla^2 \mathbf{U} - \frac{\mathbf{R}}{\phi} \tag{1.7}$$

Here, $\mathbf{U}$ is the average velocity of a fluid element in a pore. Equation (1.7) is the vector form of the macroscopic momentum equation in porous media. The

resistance $\mathbf{R}$ in equation (1.7) is obtained by applying equation (1.6) in each of the three directions of flow. The scale of the gradients defined in equation (1.7) are of the order of the representative elementary volume, and is larger than the scale of a single pore.

The term $\nabla.\left(\overline{\tilde{\mathbf{U}}\tilde{\mathbf{U}}}\right)$ on the right hand side is often called "hydrodynamic dispersion" and is an artifact of the volume average operator applied on a non-linear term. Physically, it represents transport enhancement by eddies shed from the solids of the porous medium (like the eddies shed from a cylinder in cross-flow in inertial flows); the eddies are of the size of the pore since this term represents the fluctuations over a pore-average.

For steady, constant property flow through a porous medium of constant cross-sectional area and negligible spatial acceleration and viscous forces at scales larger than the pore-scale (such as the viscous damping by a wall boundary), equation (1.7) reduces to:

$$-\nabla(\phi p) = \frac{\mu \mathbf{U}_D}{\sqrt{K}} + C\rho \mathbf{U}_D|\mathbf{U}_D| + \nabla.\left(\phi\overline{\tilde{\mathbf{U}}\tilde{\mathbf{U}}}\right) \quad (1.8)$$

Although the preceeding discussion on resistances in porous media and quantifying these resistances as functions of length and velocity scales representative of the porous medium is seemingly simple, one must be careful in employing these equations to describe the flow. Lage et al. (2005) discuss the conditions under which the description of flow using equation (1.8) are valid. Many of the common types of porous media are made of randomly distributed solids. Measuring flow quantities within the porous medium using intrusive measurement techniques is difficult unless probes smaller than the smallest pore in the porous medium are

employed for measurement. Often on-average quantities such as overall pressure-drop across the porous medium and average velocity measurements made near the exit of the porous medium are used in conjunction with equation (1.6) for computing resistances. Lage et al. note that if any of the negligible terms, such as spatial or temporal acceleration, or viscous forces near the presence of a wall exist, equation (1.8) is no longer valid for describing flow through the porous medium.

It must also be remembered that in wall-bounded porous media flows, in the near vicinity of the walls, the assumption of volume averaging technique that there are several pores in the REV might also break down, depending on the arrangement of the pores. Brinkman (1949) proposed a model that overcomes this situation by considering the force experienced by a clear fluid in the absence of solid obstructions, and added an additional drag force due to an agglomeration of solids in the near vicinty of walls. Brinkman defined an "effective viscous force" due to a boundary layer growing on the wall, which allows researchers to extend equation (1.8) all the way up to a solid boundary by adding the effective viscous force due to a wall boundary, $\mu_{eff}\nabla^2\mathbf{U}$, irrespective of whether there are adequate pores in the near vicinty of the walls to allow volume-averaging technique to be valid. The quantity μ_{eff} is referred to as the effective viscosity . As this model greatly simplifies computation of porous media flows in the near wall region, it has encountered successful application.

Despite its success, Nield (1991) notes some of the limitations of the Brinkman model, and observes that the major shortcomings of this model is its ambiguity in not defining the effective viscosity. In addition to the limitations observed by Nield, it must also be noted that the variation, if any, of hydrodynamic eddy dispersion in the vicinty of walls has not been accounted for in Brinkman's model;

in examining the literature (to be discussed in 1.4.4) it is evident that three different near-wall phenomena occur in porous media flows, and one must be careful in attributing an observed near-wall effect to a physical phenomenon.

Taking into consideration the intrinsic features of porous media flows, it is now worthwhile examining some of the experimental techniques that have been employed for characterizing flow through porous media. Of particular interest are intrusive measurement techniques outside the porous medium and the extent to which flow features inside the porous medium can be described using such measurements.

1.3 Experiments on porous media flows

der Merwe and Gauvin (1971) measured the static pressure distribution on banks of spheres. The porosity of the packed bed was 47 %. The motivation behind these measurements was to identify the inertial regime at different Reynolds numbers of flow by quantifying the location of boundary layer separation behind each bank of sphere. They discovered that the separation point was at 90° for the first bank of spheres, moving to 130° for the second and subsequent banks of spheres. Masuoka and Takatsu (2002) performed flow visualization experiments and spectral measurements to identify if spectral response of flow inside the porous medium in the inertial regime resembles that of unobstructed turbulent flow. They concluded that turbulence-like spectral behavior is observed at $Re_D \sim 10^4$. At this Reynolds number, the power spectral distribution shows the characteristic -5/3 slope in the "inertial sub-range", similar to the behavior of unobstructed turbulent flows. This indicates that eddies of different sizes are present within the pores and

energy cascade occurs in the porous medium. Having an orderely arrangement of solids, such as a regular cubic packing or a rhombohedral arrangement facilitated measurements inside the porous medium in the experiments of Merwe and Gauvin and Masuoka and Takatsu.

Disorderely porous media are more common in engineering applications, and they pose the problem of randomly distributed pores. Without apriori knowledge of pore location inside the medium, intrusive measurement techniques are nearly impossible. Seguin et al. (1998) used electrochemical probes embedded inside different types of porous media such as packed beds of spheres and foams to measure fluctuations in shear stress. They were able to obtain chaotic signals at $Re_D \sim$ 500-1000; spectral measurements obtained from these chaotic signals quantified inertial flow in porous media.

Perhaps the first direct comparison of characteristics of flow within a disorderely porous medium and that exiting the medium was made using Laser Doppler Anemometry (LDA) measurements in ceramic foams of different pore sizes by Hall and Hiatt (1996). Their experimental setup consisted of a porous duct, containing a thin and optically accessible plenum at mid-axial distance of the duct. Measurements of mean and (temporally) fluctuating components of velocity were made at the plenum as well as at the exit of the porous medium. The authors observed that the velocity profiles within and at the exit fluctuated about the mean velocity at both locations, and local jetting of fluid through the pores was observed. However, not having any upstream effects made such comparison somewhat uninteresting, since the sole discernible flow feature at both measurement locations, namely within and outside the ceramic foam, is that of random fluctuations of velocity corresponding to the random porosity variations.

1.4 Previous work on porous media flows with perturbations

1.4.1 Transport enhancement by pore-scale eddies

The focus of the present study is the effect of upstream disturbances and employing measurements outside the porous medium to quantify flow development inside the porous medium. Similar techniques employed by other researchers to study are of consideration in this section.

Niu (2005) proposed a model to evaluate eddy component of transport (eddy-dispersion) in porous media. The eddy component of transport is in many ways similar to eddy transport in turbulent flows. A simple zero-equation model for eddy transport in porous media employing the gradient diffusion hypothesis was proposed. The gradient diffusion hypothesis relates the eddy transport of a quantity to the gradient of that quantity. For instance, the turbulent transport of momentum [1]is represented as:

$$\overline{u_i' u_j'} = \epsilon_{Mi,j} \frac{\partial \overline{u_i}}{\partial x_j} \tag{1.9}$$

Here, the overbar indicates time-average component and primes indicate temporally fluctuating component of velocity vector. $\epsilon_{Mi,j}$ represents the coefficient of transport of a component of momentum in a given direction. In an analogous manner, the eddy component of transport in porous media can also be

[1] It must be noted that equation (1.9) is written so as to represent transport of three components of momentum in all three directions.

represented using the gradient diffusion hypothesis. Niu showed theoretical development demonstrating that the temporal averaging and volume averaging are equivalent, and hence, equation (1.9) is representative of eddy transport in porous media as well. If the temporal and spatial averaging were not to be equivalent, obtaining eddy transport in porous media would involve obtaining spatially fluctuating components of velocity to obtain $\epsilon_{Mi,j}$. This would involve embedding probes at several locations in the porous medium and taking measurements of velocity simultaneously at several locations, a task far more challenging than obtaining temporally fluctuating components of velocity at a location.

Experiments were conducted on a porous medium identical to the one that will be employed (discussed in section 2.3.1) in the present study. Radial transport of momentum and axial transport of thermal energy by pore-scale eddies were of interest in Niu's study. Hence, a radial gradient in velocity and an axial gradient in temperature were created, and these coefficients were measured. The radial velocity gradient was achieved by disturbing the flow using a circular plastic disc with a hole in the center. Ten hydraulic diameters downstream, the effects of the plastic disc were felt in the measured velocity profile. In the model proposed by Niu, the coefficients were assumed to be isotropic. Measurements of fluctuating components of velocity averaged over a radius corroborated this assumption, although averaging over a scale larger than the size of the pore (i.e. larger than the hydraulic diameter), but smaller than the radius may indicate otherwise.

1.4.2 Upstream half-axial gap

Quinnell (2008) reported flow measurements made using hotwire anemometry of

flow exiting a porous medium with an upstream perturbation near the walls of the test-section. The perturbation was offered by a gap extending for half-axial length of the test-section. It was discovered that the flow in the near-wall region bypassed the perturbation, and flow rates were lower in the near-wall region. Although counter-intuitive, the results from this study, like those of Niu (2005) also showed that upstream influences are persistent in the flow exiting the porous medium. It must be noted here that Quinnell's study documented flow in the near vicinity of walls of the container, where as in Niu's study, the plastic disc with the hole was placed in the core flow, away from the wall. It must also be noted that in Quinnell's study, the effects of perturbations persisted a longer streamwise distance than those of Niu's study. Neither of the two studies have quantified these effects thouroughly; the cause for the persistence of the features introduced by the upstream perturbations was not resolved.

Ganesan et al. (2009) reported results from a computational study of the same flow and geometry as that of Quinnell. Given the range of scales of the computational domain, the computation chose a "macroscopic" approach to describing the flow, employing equation (1.6) to describe the porous medium, instead of physically representing each pore and solid boundary in the computation. The values of permeability, K, and the inertical coefficient, C were obtained from the experimental data of Quinnell, since the geometries and flow parameters between the two studies were similar. The eddy dispersion was captured using the model proposed by Niu. The computational results showed that the effects of upstream disturbances were erased, and the velocity profiles obtained using as flow exits the porous medium did not show any non-uniformity, unlike the results from the experiments of Quinnell. The authors attributed the mismatch between the computational and experimental results to the computational model's assumption of

isotropy and argued that in the presence of the gap, the flow streaks into the zone of low resistance, rendering the flow anisotropic, since the eddies are stretched in the streamwise direction when jetting into the gap. Not capturing these effects in the computation was suggested as a possible reason for the model's poor performance for capturing flow with a perturbation.

1.4.3 Jet penetration through a porous medium

Having an upstream gap inside the porous medium results in flow jetting through that region because of low resistance offered by the gap. Spreading rate of this jet inside a porous medium is expected to be different from spreading rate of free jets. The spreading of free jets can be considered as though the jet is spreading through a porous medium of 100 % porosity. The other extreme situation is that of a jet impacting on a wall, a solid boundary of 0 % porosity, in which the jet gets deflected. Spreading of a jet inside a porous medium is expected to fall between these two extremes. The void spaces in the porous medium offer a path for the jet to spread through, whereas the solids that constitute the porous medium deflect the jet. Consequently, jets spreading through porous media tend to have different characteristics than either of the two situations. One can estimate that the spreading rate of jet is strongly dependent on porosity.

Niu (2005) performed experiments on a Stirling cycle regenerator made of porous medium of identical pore size and porosity as the porous medium that will be employed in the present study. Jets were introduced into the porous matrix from a cooler tube in a configuration (Figure 1.3) that is different from what will be

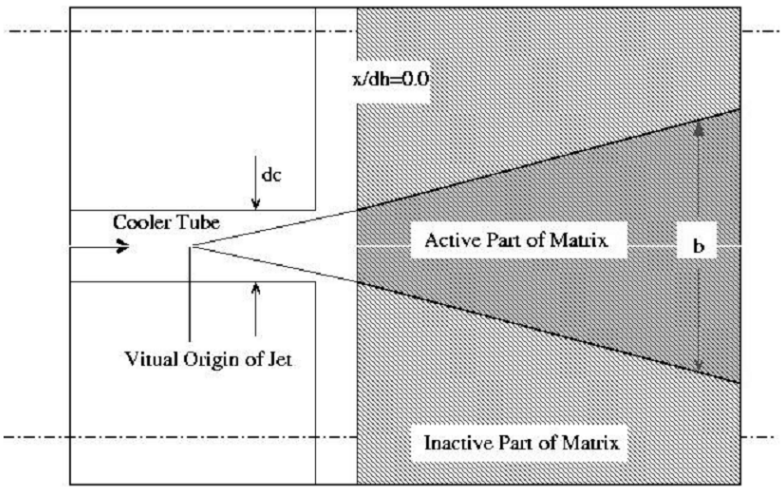

Figure 1.3: Jet penetration in high porosity porous media under oscillatory flow conditions. Adopted from Niu (2005).

employed in the present study. The objective of Niu's experiment was to quantify flow redistribution and non-uniformity in porous media in the presence of a disturbance created by a jet entering the porous matrix under oscillatory flow conditions. The results of the present study are not expected to match those of Niu's experimental results due to intrinsic differences introduced by geometry and temporal acceleration effects (in the case of Niu's study).

Based on the measurements of a jet spreading inside the porous medium, the uniformity of flow was quantified in terms of casting the fraction of area of the matrix that was "inactive" (Figure 1.3). Niu also proposed a model for the eddy transport inside the "active" porous medium, based on similar efforts for the spreading of a free turbulent jet in the absence of a porous medium. Prandtl's mixing length theory was employed in conjunction and the eddy transport was

assumed to be constant. The transport coefficient ϵ_M in the active part of the matrix was found to be about 250 - 600 times the molecular transport coefficient, i.e. kinematic diffusivity, ν.

Although this study was perhaps one of the few that discussed the growth and spreading of jets in porous media, it has its shortcomings. The extension of empirical correlations for the spreading of a free jet to that of a jet inside the porous medium without accounting for porosity is somewhat questionable. Also, it is possible that the temporal acceleration introduces effects such as weakening eddy transport when flow is temporally accelerating, which might not happen in steady flows. One of the important points of consideration in the present study is the radial location of the disturbance (a gap or a blockage) on the flow features. Literature suggests that the near-wall region in porous media requires additional care when computing flow in the region. The model proposed by Niu to compute spreading of the jet might break down in the near-wall region because it assumes that the eddy transport is a constant. While this might hold good in regions where the size of the eddies and velocity in the pore are constant (such as in the active part of the matrix in Niu's experiments), near the walls of the porous medium the eddies get constrained by the wall and the length and velocity scales may both decrease, resulting in a value of eddy diffusivity that is not constant. Nonetheless, the methods employed in Niu's study to quantify eddy component of dispersion in porous media could be applied with suitable modification in the present study in the near-wall region. This will be explained in Chapter 5.

1.4.4 Near-wall transport

Porous media studies from the literature presented so far have not examined transport in the near-wall region. This will be examined in this section. Three different physical phenomenon occur in the near wall region. The first is the presence of a wall boundary which alters the Darcy and Forchheimer resistances since these resistances are representative of a porous medium free of boundary effects. The model proposed by Brinkman (1949) attempts to overcome this difficulty by defining an effective viscous force, which is a sum of the Darcy resistance and the viscous drag force experienced by a clear fluid in a channel. However, as noted by Nield (1991) the exact value of this effective viscosity remains ambiguous. Nield observes that researches tend to cast this effective viscosity as the dynamic viscosity divided by the porosity resulting in a highly viscous region near the wall boundary. The second phenomenon that researchers have observed in the near wall region is that flow tends to ooze to the near wall region, and this has been attributed to the porosity being high on average near the wall before falling back to zero at the wall (impermeable boundary). Figure 1.4 illustrates this channeling effect. The third physical phenomenon is the variation of eddy component of dispersion in the near wall region. One must be careful in making the distinction between the three physical phenomena: the first is observed in all porous media flows. The second is an effect which arises when porosity varies near the wall (such as stacking a regular arrangement of spheres). The third is an inertial effect as it occurs only when eddies are shed from the solids in the porous medium. Distinguishing these three effects is inherently difficult, but it must be remembered that they represent different physical phenomena and careful consideration is required before attributing a higher velocity near the wall to any of these phenomenon.

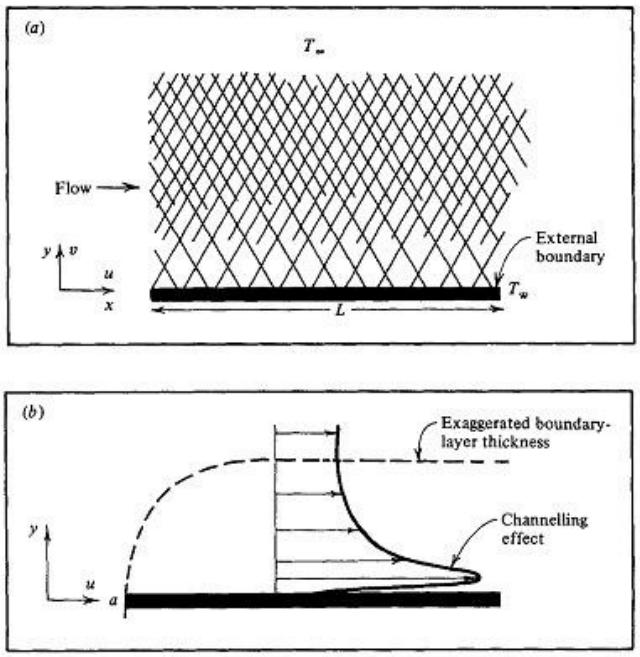

Figure 1.4: Near-wall channeling of flow and variable porosity. Figure adopted from Vafai (1984).

Hunt and Tien (1988) made some efforts in distinguishing the porosity variation near the wall and the damping of eddy dispersion by the wall boundary for packed beds, although the near-wall channeling was also considered as a "non-Darcian" effect, i.e. one that is not observed in the low-Reynolds number flow regime, which is questionable, as one would expect that regardless of the Reynolds number, flow migrates to regions of low resistances, and this migration occurs in the viscous (Darcy) as well as the inertial (Forchheimer) regimes of flow. An example of near-wall channeling in the Darcian regime was studied by Beavers and Joseph (1967) who observed an increase in mass flow near the wall in the Darcian regime. Hence, it is incorrect to attribute near-wall channeling to be a "non-Darcian" effect.

Adnani et al. (1995) reported numerical analysis of thermal transport in packed

beds of low porosity ($\sim$ 50 %). Their study, like that of Hunt and Tien (1988) did not explicitly distinguish the wall-damping of the eddies from the near-wall variation in porosity; rather, they observe that eddies become less tortuous near the wall because of the increase in porosity near the impermeable boundary. This raises a question: hypothetically, if the porous medium were made of uniform porosity, will the wall suppress the size of the eddies and make them weaker?

Amiri and Vafai (1994) performed computation of thermal transport in low porosity media taking into account variation of porosity near the wall. Their model for thermal transport enhancement by eddies factored in the porosity variation, and in some sense can be considered a variable thermal dispersion model. However, they did not model the hydrodynamic dispersion similarly, and their model lacks physical reasoning, since the eddies that are responsible for momentum transport are also responsible for transport of thermal energy, and if thermal dispersion is modeled by a damping function near the wall, the momentum dispersion must also be damped similarly. The authors do not provide any support for not modeling hydrodynamic dispersion term correctly.

Vafai (1984) performed computation of packed beds accounting for near-wall variation in porosity. It was argued that porosity was an exponential function of the distance away from the wall in packed beds based on previous measurements. The computed profile did not account for eddy-component of dispersion, and yet showed good agreement with measurements for packed beds. It is possible that in packed beds, because of the low values of porosity (less than 70 %), the eddy transport component is not effective even in the core of the porous medium and eddies might get suppressed even in the core.

Although a thorough investigation of near-wall phenomena is available for packed

beds, the conclusions drawn from these studies cannot be directly applied to near-wall phenomena in high-porosity media where the pore-scale fluid dynamics is vastly different.

McFadden (2005) noted that thermal transport in the near wall region might be poor as a result of damping of near-wall eddies. In an attempt to quantify the eddy component of dispersion, temperature measurements were taken within the porous matrix, generated by a thermal wake. The spreading of the wake was attributed to the enhanced transport due to pore-scale eddies. This 'indirect' method of obtaining eddy transport was compared to the 'direct' method of obtaining eddy component of dispersion from the experiments of Niu (2005). Both the direct and indirect measurements agreed with each other, indicating that measurements made as the flow exits the porous medium can be representative of measurements inside the porous medium.

McFadden suggested an exponential decay of eddy coefficient of dispersion from the core of the porous matrix to the wall. Qualitatively, the value of effective diffusivity (sum of molecular and eddy component of dispersion) should be equal to the molecular diffusivity at the wall, and must approach the eddy dispersion value in the core; one way to intepret this variability is that in the core of the porous matrix, pore-scale eddies are active participants in transport and hence the diffusivity of a quantitiy is high in the core of the matrix. As the wall is approached, the eddies get weaker and transport is vastly different in this region, and upon getting closer to the wall, the transport is achieved solely at molecular scales. McFadden obtained a model for the eddy dispersion variation near the wall by matching the unknown coefficients of the exponential decay function with a measured temperature profile. The ratio of effective conductivity, k_{eff}, which is

due to eddy dispersion, to thermal conductivity of the fluid, k, was presented as a quantity to gage the eddy activity in the matrix, and its variation near the wall was cast as:

$$\frac{k_{eff}}{k} = C_1 + C_2 e^{-n(1-r)} \tag{1.10}$$

where, the distance away from the wall is r (a dimensionless quantity). The exponent n was referred to as "shape parameter" determining the thickness of the wall-boundary layer and assumed to be 25 from the measurements of temperature profile. It was noted that larger values of n led to a thinner boundary layer. The constants C_1 and C_2 were defined as:

$$C_1 = \frac{e^n k_{eff,\infty} - k}{e^n - 1} \tag{1.11}$$

$$C_2 = -\frac{e^n (k_{eff,\infty} - k)}{e^n - 1} \tag{1.12}$$

Here, the eddy dispersion conductivity at the core is indicated as $k_{eff,\infty}$. At the wall, the dimensionless radius equals one, and the ratio of eddy dispersion conductivity to fluid thermal conductivity equals one. Far away from the wall, and at the core, this ratio approaches $\frac{k_{eff,\infty}}{k}$. This model suffers from two limitations: the assumption of an exponential decay of eddy dispersion lacks physical intuition, since there is no analytical constraint that forces $\frac{k_{eff}}{k}$ to take this exponential form. The second, and more serious limitation of this model is that it requires apriori knowledge of the boundary layer thickness to fix the value of the "shape

parameter", n. When the value of n approaches zero or infinity, leading to situations where the wall boundary layer is extremely thick or thin the ratio of eddy dispersion conductivity to thermal conductivity remains inderminate, a situation which is clearly non-physical.

1.5 Summary of previous work

The objectives in examining the literature were to review methods employed to study porous media flows, particularly the ones that have been subject to perturbations, leading to the development of a jet or a wake spreading inside the porous medium. Similar studies have attempted to quantify the development of a jet, drawing support from the spreading of free jets. Quantifying near-wall flow in porous media has remained a muddy point, and the physics of flow in this region is not clearly understood. Although several researchers have performed thorough parametrization of near-wall flow phenomena in packed beds, drastic differences between flow through high-porosity media and that through packed beds are restricive in extrapolating results. The literature also supports the hypothesis that flow exiting the porous medium sheds insight on the nature of flow inside the porous medium, a fact that encourages intrusive measurements as flow exits the porous medium to describe fluid dynamics within the porous medium.

1.6 Scope of the present study

The objectives of the present study are to investigate porous media flows subjected to disturbance, namely, an upstream half-axial gap and a blockage. The influence of the radial location of the disturbance will be studied by positioning the disturbance in the core flow, where "wall-effects" are negligible, and near the wall where such effects are expected to contribute to additional flow distortion. As noted earlier in section 1.4.4, it is of interest to understand and isolate channeling of the near-wall flow due to high-porosity in this region from the effects of damping of eddies by the wall, an effect that is often coupled with the higher porosity in this region.

It was also pointed out that measurements of flow inside porous media have proved to be difficult. For a thorough understanding of the effects of disturbances, profiles of quantities such as velocity at multiple axial locations inside the porous medium will prove valuable. However, such measurements are beyond the scope of this study because of the geometry of the porous medium and the disturbance would pose considerable difficulty in traversing probes. From the experiments of Niu, it was demonstrated that careful and systematic measurements of flow immediately downstream of the porous medium can document flow characteristics inside the porous medium. This approach will be followed in the present study to address the questions concerning the effects of upstream disturbances.

Chapter 2

Experimental methods

2.1 Overview

Porous media flows subject to upstream perturbations that extend for half-axial length of the test-section have not been studied in the literature so far. Primary difficulties in studying such a flow arise from the broad range of scales present in the porous medium. Also, if the perturbations extend half-axial length, discerning the evolution of flow features, such as the spreading of a jet or a wake inside a porous medium would involve making measurements inside the porous medium. A typical wire-mesh screen porous medium has a complex geometry with random distribution of pores; thus, traversing probes inside the porous medium is rendered nearly impossible. As pointed out in Chapter 1, researchers have often tried to study porous media flows by taking measurements external to the porous medium at the exit, and correlating the flow features at the exit to upstream features of the flow. Another difficulty that is posed by the structure of the porous medium

with randomly distributed pores is the low "signal-to-noise" ratio. Consider flow through a test-section with random variations of porosity because of the structure of the porous medium. Regions of high porosity might present opportunities for jetting to occur, as flow has the tendency to travel through paths of least resistance. The converse of this is true for regions of low porosity, through which flow avoids passing. Hence, random variations in porosity introduce considerable amounts of noise in the measurements, and discerning flow-features such as a jet or wake introduced by upstream perturbations from jets or wakes that develop due to arbitrary variations of porosity is difficult. Lastly, for low speed flows such as the ones of interest in the present study, statistical uncertainty in velocity measured using hotwire anemometry (to be discussed in sections 2.5.1 and 2.5.3) tends to be large (as much as $\sim$ 10-15 %), and obtaining good signal-to-noise ratio can be difficult for such low speed flows.

2.2 Methodology

The effects of upstream perturbations on flow through a porous medium are of interest in this present study. Velocity profiles of flow subject to an upstream gap, resulting in the evolution of a jet inside a porous medium, or an upstream blockage, resulting in the evolution of a wake inside the porous medium, will be observed to discern the effects of the presence of an upstream gap and blockage on flow features, and, consequently, transport phenomenon in porous media. As discussed earlier in this chapter, structural features of the porous medium prevent traversing a probe to acquire profiles of velocity. Further, it was also pointed out that random variations of porosity introduce noise in the meaurement, making it

difficult to isolate a jet or a wake that may persist due to an upstream gap or blockage from "local" jets or wakes that develop as a result of regions of high or low porosity distributed within the porous medium.

To this end, velocity profiles are obtained from hotwire traverses at the exit of the porous medium; to isolate features that may exist at the measurement plane as a result of upstream perturbations (signal) from flow features due to local variations of porosity (noise), the following procedure is adopted: the upstream perturbation (gap or blockage) occurs at several circumferential locations. The local perturbations in porosity are randomly distributed. Hence, measurements taken at several circumferential locations can be correlated with the location of the upstream perturbation. This will be illustrated in Section 3.1. On moving from one radial or circumferential location to the next at the measurement plane, flow features that are due to porosity variations will not be correlated due to the random nature of porosity variation; however, if at two circumferential or radial locations on the measurement plane, the flow had been subjected to the same kind of perturbation upstream, features that correlate with the upstream perturbation will be observed at both locations, and velocity profiles at these locations will be similar.

Also, experiments on unperturbed flow through a porous medium can provide valuable information on flow features in different regions of the flow. These experiments can serve as a base for comparison against the experiments with upstream perturbations. If the flow were to be distorted as a result of perturbations, the effect of perturbations on flow can be discerned direcetly from such a comparison to draw meaningful conclusions about the perturbed flow.

In essence, some of the difficulties posed by the nature of the porous medium and

low-signal to noise-ratios that are characterisitics of this flow can be overcome by making careful and systematic set of measurements as flow exits the porous medium. By correlating the flow features at the exit to the upstream perturbation, and by comparing these features to unperturbed flow through the porous medium, effects of perturbations and the nature of flow subject to perturbations can be documented.

2.3 Description of the experimental cases

Three sets of experiments have been considered: Unperturbed flow, upstream near-wall perturbations, and upstream core-flow perturbations. These cases are also summarized in Tables 2.1 and 2.2.

2.3.1 Unperturbed flow (no upstream gaps or blockages)

Velocity profiles are acquired for flow through a porous medium without any upstream disturbances. The porous medium used in the present study is identical to the pattern porous medium employed in previous research at the Heat Transfer Laboratory, and is typically fabricated by stacking metal screens in a circular duct. The screens used in the present set of experiments are made of stainless steel wire. Two hundred metal screens were stacked against each other so that they formed a snug fit against the walls of the test-section. The diameter of each of the screen is 190 mm. The screens are made of metal wires of diameter (D_w) 0.81 mm, and have a wire spacing of 4 per inch, i.e. the distance between two wires in the square mesh is 0.25 inch (6.35 mm). A more common length scale of

the stacked-screen porous medium is the hydraulic diameter D_h, defined as:

$$D_h = \frac{\phi D_w}{1-\phi} \tag{2.1}$$

Here, ϕ is the porosity. The porosity of the screen packing used in all experiments was 90%. The hydraulic diameter of the porous medium was 7.29 mm; this length scale is often considered as the average pore-diameter, the characteristic length scale of the porous medium in the literature[1]. The ratio of diameter of the screens to the hydraulic diameter is 26.

The flow Reynolds number can be defined based on the hydraulic diameter as the characteristic length-scale, as:

$$Re_D = \frac{U_D D_h}{\nu} \tag{2.2}$$

The characteristic velocity scale is the Darcy velocity, U_D. In a two-dimensional sense, the velocity obtained from hotwire traverses can be integrated over the area of cross-section, and this can be written as:

$$U_D = \frac{1}{A}\int_A U dA \tag{2.3}$$

The Darcy velocity of the experiments was 0.45 m/s, corresponding to a Reynolds number of 200. It was noted earlier in Section 1.3 that this Reynolds number

[1] It must be noted here that the spacing between the wires in the wire-mesh screen is 6.35 mm and it is arguable that this is a better representation of the pore-diameter. However, it must be remembered that the screens have been cut randomly, and stacked so as to avoid jetting, and hence, equation (2.1) is a more reasonable "on-average" pore-diameter.

corresponded to an inertial regime with flow features bearing similarity to unobstructed turbulent flow. The inertial regime was characterized by eddy-shedding from the metal wires of the porous medium, resulting in transport enhancement by the pore-scale eddies referred to as eddy dispersion. Similar behavior is expected in the experiments involving unperturbed flow.

Table 2.1: Test conditions for unperturbed flow

Screen diameter	190 mm
Number of screens	200
Porosity	90 %
Hydraulic diameter, D_h	7.29 mm
Darcy velocity, U_D	0.45 m/s
Reynolds number, Re_D	200
Axial length of the test-section	314 mm ($\sim$ 42 D_h)
Measurement plane	1 D_h downstream of the last screen

2.3.2 Upstream near-wall perturbations

In this experimental case, the near-wall region of the flow was perturbed for an upstream distance of twenty-one hydraulic diameters, and flow was allowed to travel the same distance downstream through the porous medium without any perturbations. One-hundred screens of diameter 190 mm (identical to the ones used for the experiments involving unperturbed flow), and one-hundred screens of diameter 183 mm were used in the upstream half of the test section. The small

diameter screens were cut from the large diameter screens, so that the mesh-spacing, wire-diameter and porosity of the small diameter screens were the same as those of the large screens. The large diameter screens were stacked so that they formed a snug fit against the walls of the circular duct which holds the screens. The small screens created a gap between the screens and the walls of the test-section, which extended an axial distance of 157 mm ($\sim$ 21 D_h). Four cardboard spacers 157 mm (21 D_h) long, 10 mm (1.4 D_h) wide and 4.2 mm (0.5 D_h) radially thick were used to hold the small screens in place and prevent them from slumping. The spacers perturbed the near-wall flow by acting as a blockage and allowing a wake to develop downstream of the spacers. These spacers occupied approximately 6-8% of the total gap cross-sectional area. The spacers and the gap are referred to as 'near-wall perturbations'. Figure 2.1 is a schematic of the experimental setup showing the perturbation locations with respect to the flow direction and measurement location.

2.3.3 Upstream core-flow perturbations

The core-flow experiments were conducted to identify how the effects of the perturbations differ with radial location of the perturbations. In these experiments, perturbations similar to the ones described in 2.3.2 are placed in the 'core' of the porous matrix. The core is identified as a region located sufficiently away from the walls of the test-section. Two cases of core-flow perturbations were considered. The characteristic length-scale of the core-flow perturbations and their upstream extent(axial distance for which the flow is perturbed) are chosen so as to facilitate a fair comparison between these experiments and the near-wall perturbation experiments. The core-flow disturbances are illustrated in figure 2.2

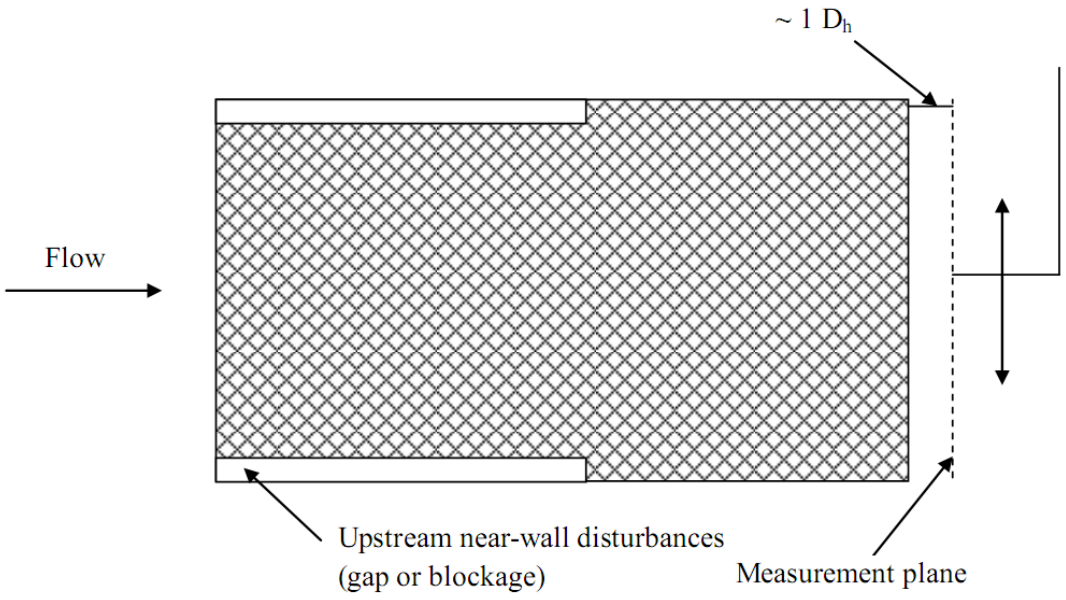

Figure 2.1: A schematic of the experimental setup of the near-wall perturbation experiments

Jet spreading through the core of the porous matrix

One-hundred circular screens of diameter 190 mm (identical to the ones used in the unperturbed flow experiments) with a 1 cm (1.4 D_h) hole at their center were stacked followed by one-hundred screens of diameter 190 mm without a center hole formed the test-section. This corresponded to a distance of twenty-one hydraulic diameters of travel through screens with center-holes (upstream core-flow perturbations) followed by twenty-one hydraulic diameters of travel through screens without center-holes. The center-holes create an alternate low-resistance

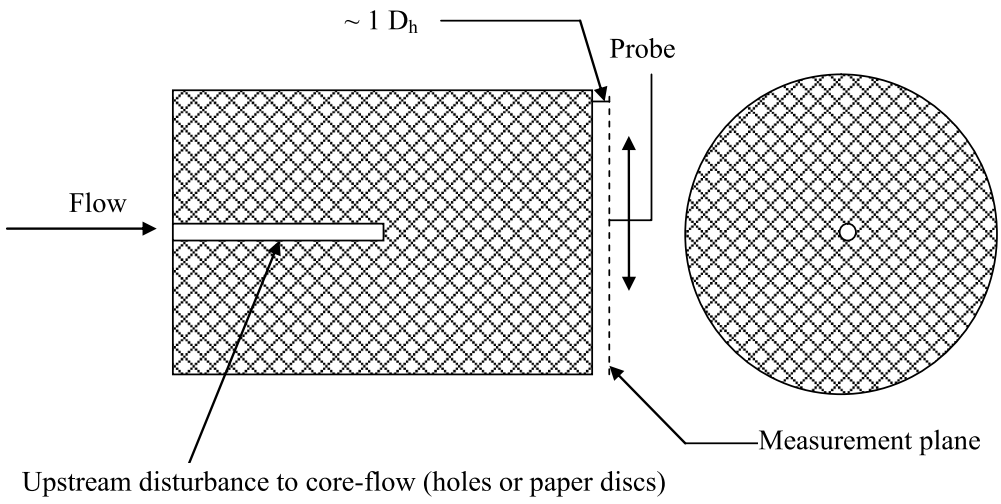

Figure 2.2: A schematic of the experimental setup of the core-flow perturbation experiments

path for jetting, equivalent to the gap in the near-wall perturbation case.

Wake spreading through the core of the porous matrix

This case is similar to the one with a jet spreading through the core, with one-hundred circular screens of diameter 190 mm with a 1 cm (1.4 D_h) paper disc at the center of each screen followed by one-hundred screens of diameter 190 mm without discs. The layers of paper discs at the center act as a blockage and create a region of high-resistance. Flow avoids this region, and a wake develops downstream.

Table 2.2: Test conditions for experiments involving perturbations

Quantity	Near-wall	Core-flow
Screen diameter	190 mm (downstream 100 screens), 183 mm (upstream 100 screens)	190 mm
Porosity	90 %	
Hydraulic diameter, D_h	7.29 mm	
Axial-length of the test-section	314 mm ($\sim 42\ D_h$)	
Characteristic scale of perturbations	Annular gap of thickness 4.2 mm, 4 blockages of thickness 4.2 mm each	Holes and blockages of diameter 1 cm
Streamwise extent of the upstream perturbation	157 mm ($\sim 21\ D_h$)	
Darcy velocity, U_D	0.45 m/s	
Reynolds number, Re_D	200	
Measurement plane	1 D_h downstream of the last screen	

2.4 Description of the flow facility

The experiments were conducted at the Heat Transfer Laboratory, University of Minnesota. Figure 2.3 is a schematic of the steady-flow test facility. A Dayton 3N669 blower of 5 hp capacity delivers a steady flow of air to the test-section. The flow-rate of air can be adjusted using a Magnetek frequency inverter. Appropriate flow conditioning is required to ensure that flow entering the test-section is uniform. This is achieved using soda-straw flow straighteners that are packed within the flexible duct that delivers air to a Meriam 50MC2-4 Laminar Flow Element (LFE). This flow meter has a rated uncertainty of 0.86 % of the reading. The LFE requires a long upstream straight duct (of $\sim 50\ D_h$) so as to maintain a laminar profile at inlet. A Dwyer inclined manometer of resolution 0.5 mm (0.02 inches) of water is connected across the LFE. The flow rate can then be obtained by using the manufacturer-specified pressure drop vs. flow rate curve for the LFE. The downstream duct from the LFE has a different diameter than the test-section. Thus , a diffuser packed with wire-mesh screens is used. Flow then enters the test-section, which consists of a circular duct, packed with the porous medium discussed in section 2.3.

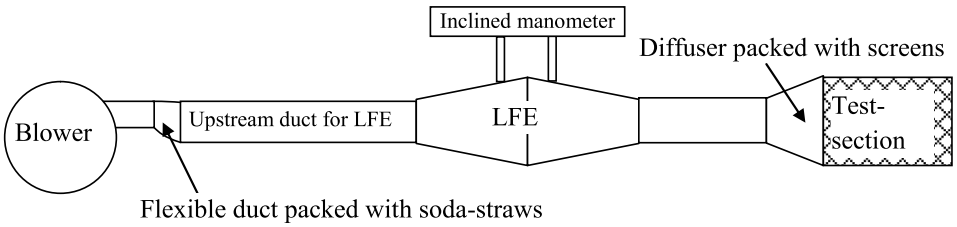

Figure 2.3: A schematic of the test-facility

2.5 Experimental techniques

2.5.1 Hotwire anemometry

Measurements of time-averaged velocity were taken using constant-temperature hotwire anemometry (CTA). Figure 2.4 is a schematic of a typical constant temperature anemometer. A constant temperature hotwire anemometer consists of a Wheatstone bridge electrical circuit. A sensor consisting of a metal wire is placed in the flow, and current is passed through the wire. The wire has a known resistance vs. operating temperature characteristics. This constitutes one branch of the Wheatstone bridge. A "control resistor" constitutes the other branch of the bridge, which can be adjusted to keep the bridge in balance when the wire is at the pre-determined operating temperature. As a result of resistance heating, the wire temperature changes from that of the flow temperature, causing the occurrence of convective heat transfer from the surface of the wire to the ambient fluid. If the wire temperature drops, producing an out-of-balance bridge voltage. The D.C. differential amplifier senses this out-of-balance voltage and, in order to bring

the bridge to balance, sends more current through the wire, increasing the temperature and resistance of the wire. In principle, an output voltage is produced by the anemometer which can be related to the rate of heat transfer from the wire, and, implicitly, the flow velocity when the fluid properties are known. The anemometer must be calibrated under conditions of known velocity to establish the relation between voltage output of the bridge and the velocity.

2.5.2 Instrumentation and signal conditioning

Velocity measurements were acquired using a TSI 1211-T1.5 Platinum coated Tungsten wire sensor. Figure 2.5 is an image of this sensor showing its critical dimensions. A TSI 1051 constant-temperature anemometer bridge was used to obtain analog voltage signals, which were digitized using an Agilent 34970A multimeter and National Instruments Benchlink DataLogger data-acquisition software. The sampling frequency was chosen by setting the integration time of the digitizer. Integration time is the period of time, during which the instrument continuously measures the input signal; the measured signal is then integrated over the integrating time, and the digitizer produces an output voltage. This is somewhat analogous to setting a sampling frequency. If the integration time is too small, the digitizer samples rapidly and acquired signals may not be statistically independent. Hence the integration time (and consequently, the sampling frequency) is chosen to be slower than the slowest eddy passage frequency. This condition is important to ensure that the voltage signals measured and "held" by the multimeter during the integration time are statistically independent of each other. (Conversely, if sampled at a frequency higher than the eddy passage frequency, two signals acquired may not represent the actual flow velocity and may

correspond to that of a single large eddy passing past the probe.) The eddy passing frequency can be computed from Strouhal number, which is a dimensionless number indicating the relative magnitudes of time-scale of convection of eddies past the probes and time-scale of eddy shedding. Alternatively, it can be defined as the ratio of frequency of eddy-shedding in the flow, f, against frequency of eddy passage past the probe, as follows:

$$St = \frac{fL}{U} \tag{2.4}$$

The characteristic velocity, U and the characteristic length scale, L were chosen to be the Darcy velocity, U_D, and the hydraulic diameter, D_h, respectively. Using a Strouhal number of 0.2, the lowest eddy passage frequency was estimated to be of the order of 15 Hz. The integration time of the Agilent 34970A is specified by power-line cycles. Following are the available sampling rates given in terms of power line cycles (PLC): 0.02, 0.2, 1, 100 and 200, where 1PLC = 1/60 seconds. An integration time of 200 PLC was chosen, corresponding to a frequency of 3 Hz, which is well below the eddy passage frequency.

Profiles of velocity were obtained by mounting the hotwire sensor on a National Aperture MM-4M-EX-140 MicroMini motorized stage and a MC-CQ motion controller operated by FAULHABER motion manager software. The axial location of the measurement plane was one hydraulic diameter from the last screen of the porous medium. Two different step-sizes were used to traverse the probe radially: 0.24 mm steps for a distance of 10 mm from the wall ($\sim 1.4\ D_h$) for finer resolution in the near-wall region, and 1.0 mm steps for the remainder of the traverse. The uncertainty in locating the wall of the test section was estimated to be of the

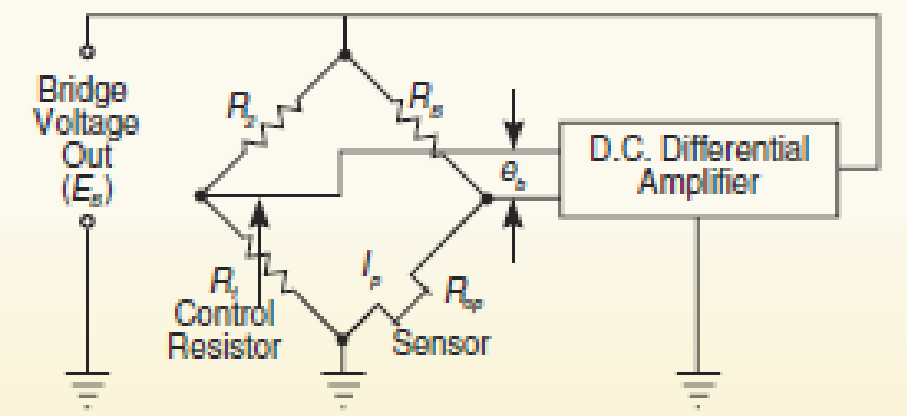

Figure 2.4: Schematic of a constant temperature anemometer (Hotwire catalog, Thermal Anemometry Systems, TSI Inc., 2008)

order of 0.5 mm. Although the traverse is capable of resolving distances finer than 0.5 mm, the wall was located by visual inspection. Repeatability of the velocity profiles obtained over a span of few days, though not the ideal method to gauge the wall position, was used as a means to verify that the wall could be located to within 0.5 mm, and that the profiles are repeatable over a short time interval. Figure 2.6 is a layout of the instrumentation employed for the measurement.

2.5.3 Hotwire calibration

The hotwire anemometer produces a voltage signal that is representative of the velocity. However, to get the velocity from the voltage signals, calibration must be performed. This involves the placement of the sensor in a flow-field of known velocity, and establishing the relationship between voltage and velocity using empirical curve-fitting procedure of the obtained voltage and velocity data.

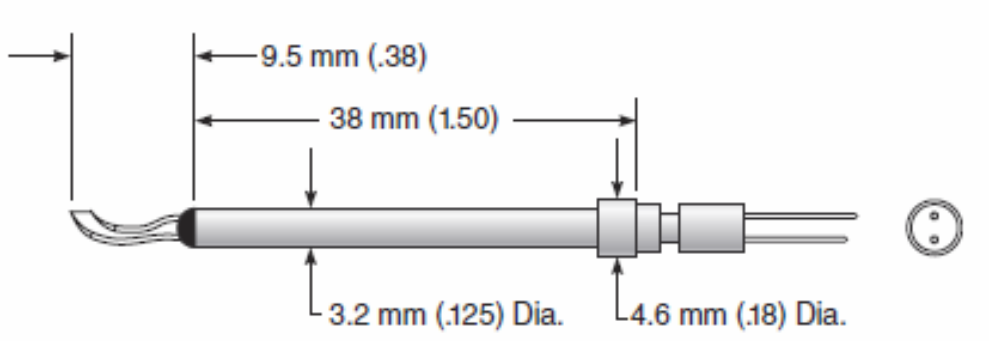

Figure 2.5: TSI 1211-T1.5 sensor and its dimensions (Hotwire catalog, Thermal Anemometry Systems, TSI Inc., 2008)

The calibration rig at the Heat Transfer Laboratory was fabricated by Wilson (1970). Figure 2.7 is a schematic of the calibration rig. Compressed air enters the rig and is conditioned by baffles and flow straighteners before passing through an elliptical contraction. Calibration of two different ranges of velocities can be performed in the rig: calibration with velocities up to 2 m/s can be done by placing the probe in the inner chamber. Static pressure at the probe location is measured using pressure taps and a Dwyer Model 1430 Microtector micro-manometer of resolution 63 μ m (0.0025 inches of water), facilitating calibration in the low velocity range.

Velocities expected in the present experiments are in the range of 0.2 to 1.5 m/s. Calibration was performed over the velocity range of 0.14 to 2 m/s. During the calibration, the differential pressure was recorded using static pressure taps and a micro-manometer and the temperature of the flow was recorded using a Resistance Temperature Detector.

King's law is often employed to express velocity as a function of voltage for the

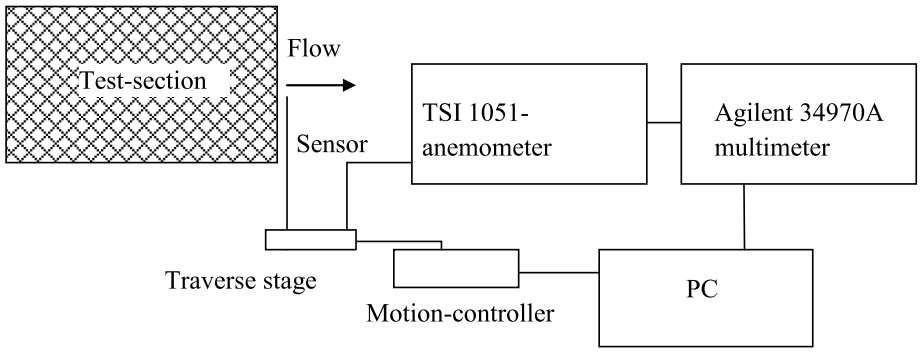

Figure 2.6: Schematic of the instrumentation used for data-acquisition

anemometer. It is of the form:

$$U^n = AE^2 + B \tag{2.5}$$

Here, U is the velocity and E is the voltage, A, B and n are curve-fitting parameters. The exponent 'n' often equals 0.5 (for King's law), although other values have been found to fit the data better. However, at low velocities, the validity of King's law breaks down and polynomial curve-fits tend to fit the data better. Heat transfer by natural convection from the hotwire sensor is a possible reason for King's law to perform poorly at low velocities. (It must be noted that King's law is a simplified expression obtained by equating the convective heat transfer by forced convection from the surface of the hotwire sensor to heat flow into the sensor by resistance heating.) Equation (2.6) relates the voltage and the velocity by a fourth-order polynomial fit:

$$U = -18.988E^4 + 180.35E^3 - 631.42E^2 + 973.65E - 560.61 \tag{2.6}$$

Figure 2.8 shows the velocity vs. voltage data and the fourth-order polynomial fit. The goodness of the fit was found by using the curve-fit equation to predict the velocity for a given voltage, and comparing the predicted velocity to the measured velocity obtained from the differential pressure measurement. The percentage difference between the measured velocity and predicted velocity using curve-fit is calculated as:

$$\%difference = \frac{|U_{measured} - U_{predicted}| \quad x \quad 100}{U_{measured}} \tag{2.7}$$

The percentage difference in the predicted velocity against the measured velocity during calibration can be related to the goodness of the fit. It can be seen from Figure 2.9 that the fourth order polynomial fits the data better than the power-fit, equation (2.5) for several values of the exponent 'n', and curve-fitting errors in the velocity range of interest, i.e. 0.2 m/s to 1 m/s, are of the order of 5 % or less for the fourth-order polynomial fit.

2.5.4 Estimation of uncertainty

Estimation of uncertainty in hotwire measurements is typically performed by discretely sampling a large number of statistically independent voltage signals during the calibration of the sensor, computing the standard error in the voltage measurement and propagating the standard deviation in voltage measurement using the calibration curve-fit to obtain the standard error in velocity measurement at a confidence interval using the Root-Sum-Squares method, as follows:

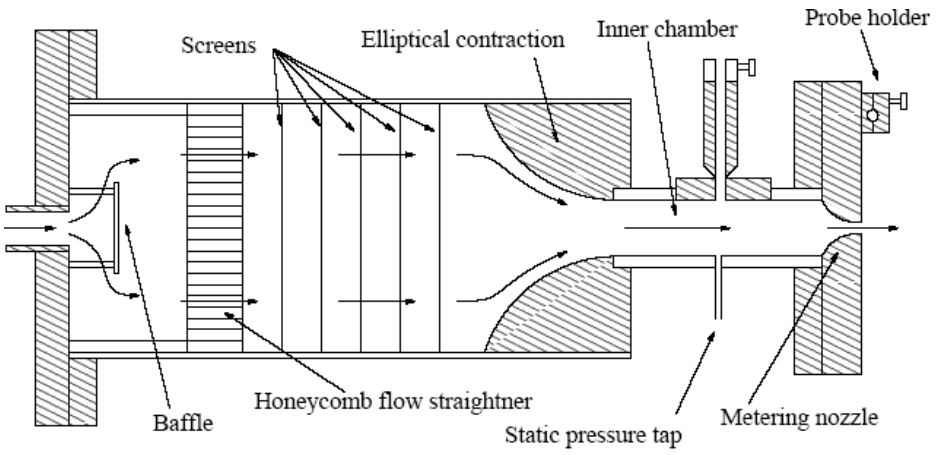

Figure 2.7: A schematic of the calibration rig

If U, the measured variable, (such as velocity) is dependent on a number of independent variables, such that U=U(X_1, X_2, X_3,...), then, the standard error in velocity, σ_U is given by:

$$\sigma_U = \sqrt{\left(\frac{\partial U}{\partial X_1}\sigma_{X1}\right)^2 + \left(\frac{\partial U}{\partial X_2}\sigma_{X2}\right)^2 + \left(\frac{\partial U}{\partial X_3}\sigma_{X3}\right)^2 + ...} \tag{2.8}$$

Here, σ_{X1}, σ_{X2}, σ_{X3} etc. are the standard deviations in measuring independent variables. Using equation (2.6), the standard deviation in measuring velocity, propagated from standard deviation in measuring voltage is given by:

$$\sigma_U \approx (-75.952E^3 + 541.05E^2 - 1262.84E + 973.65)\sigma_E \tag{2.9}$$

Using a 95 % confidence interval and student's t-distribution, the uncertainty in velocity measurement is given by:

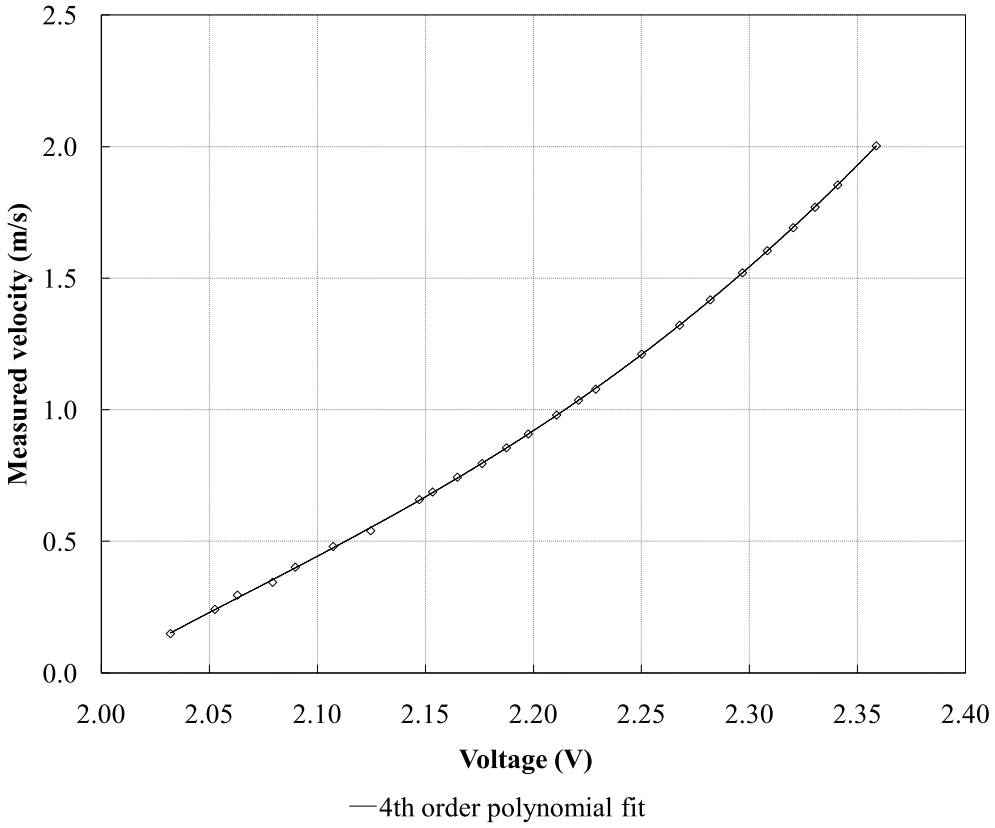

Figure 2.8: Measured velocity plotted against the measured voltage, with fourth-order polynomial fit

$$\Delta U = \pm \frac{t\sigma_U}{\sqrt{N}} \tag{2.10}$$

Here, N is the number of statistically independent samples. Although statistically rigorous, this method alone is not a good indicator of uncertainty, as it eliminates other sources of uncertainty in the measurement, such as errors in curve-fitting, instrument bias in reading the voltage signal accurately, repeatability of the experiment, and the ambient environment conditions such as the temperature and humidity variations during the time-interval between calibration and the actual

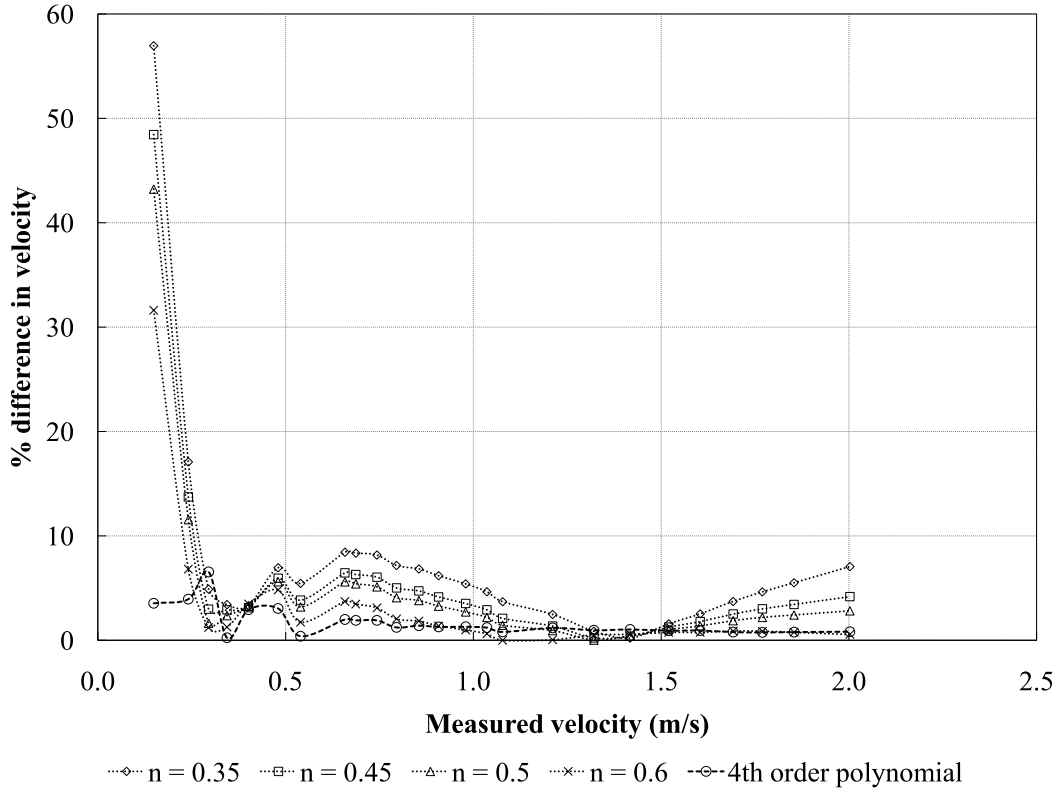

Figure 2.9: Goodness of the curve-fits for the range of velocities considered during calibration

experiment. While it is possible to account for some of these factors rigorously in the uncertainty of velocity measurement, quantifying the effects of several of these factors may turn out to be impossible. Nonetheless, to obtain an estimation of statistical uncertainty in measurements, this approach is followed. To gather further confidence in the measurements, the measurement technique is qualified by taking velocity profiles in a known flow field, which will be explained in section 2.6.

The largest standard deviation in voltage measurements is of the order of 0.001

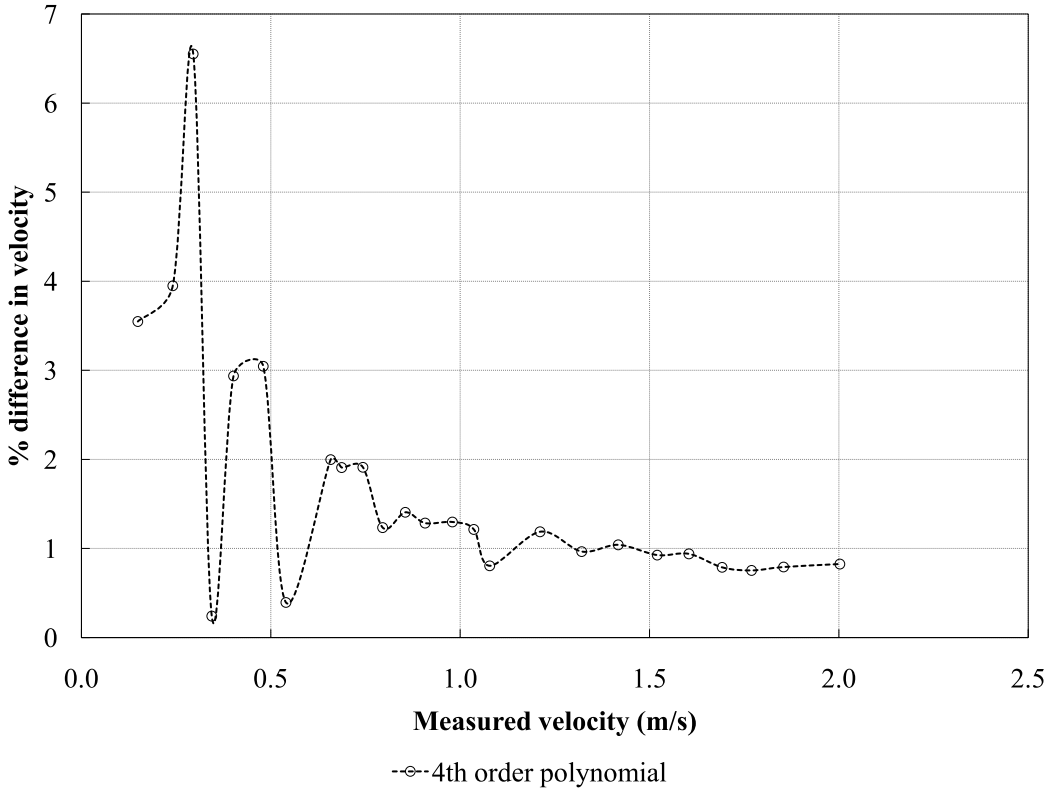

Figure 2.10: Goodness of the 4th order polynomial fit for the range of velocities considered during calibration

Volts, obtained at the lowest velocity during calibration, $\sim$ 0.14 m/s. Using equations (2.9) and (2.10), the relative uncertainty in measuring velocity is of the order of ± 1 % [2].

Ambient temperature and humidity were recorded during calibration and measurement using a hand-held hygrometer with a built-in thermocouple probe. The temperature changes were of the order of 1 %, which resulted in a velocity change of 4 %. The humidity variations during the course of the experiment were of the order of 5 %. No corrections have been performed to the hotwire signal to correct

for humidity changes. Taking into account the statistical uncertainty, and the temperature differences over the course of measurement, the uncertainty in the velocity measurement is estimated to be 5 %.

2.6 Qualification of measurements: Unperturbed flow experiments

As discussed earlier in section 2.5.4, rigorously quantifying all sources of uncertainty and propagating them into the uncertainty in velocity measurements using equation (2.8) can be difficult if the dependence of velocity on independent variables is unknown. To overcome this difficulty, and also to qualify the measurements in a situation that mimics the actual set of experiments, the hotwire sensor was traversed to obtain velocity profiles as flow exits the porous medium without any upstream perturbations, as described in section 2.3.1. These profiles were integrated to obtain the volumetric flow-rate, which could be compared to an "absolute" measurement of volumetric flow-rate from the Laminar Flow Element. As described earlier in section 2.4, the Laminar Flow Element is capable of accurately measuring volumetric flow rates and uncertainties associated with volume flow-rate measurement using the LFE are typically low. By conservation of mass, the integrated velocity profiles should give a volumetric flow-rate that matches the volumetric flow-rate measured using the LFE.

The porous medium was assembled by stacking 200 screens of diameter 190 mm

[2] It must be noted that the relative uncertainty is defined as $\frac{\Delta U x 100}{U}$, where U is the velocity at the calibration point, and ΔU is the absolute uncertainty at that calibration point. In the example considered, U is 0.14 m/s and ΔU is 0.0014 m/s

forming a snug fit with walls of the test-section; this ensures that there are no gaps or blockages that perturb the flow. The screens were stacked so that the pores were randomly distributed. This was achieved by rotating adjacent screens approximately 45 degrees from each other, so that the wires and the pores between two adjacent screens do not align with each other. Such an assembly is to prevent jetting of fluid through a "channel" created by an orderly alignment of pores from neighboring screens. Velocity profiles were obtained at the exit of the test-section at two radial lines. These profiles are shown in Figure 2.11. The profiles were integrated over the respective radius to get a volumetric flow-rate corresponding to each radial line, and this was compared to the flow-rate measured using the Laminar Flow Element. These values are summarized in Table 2.3

Table 2.3: Comparison of volumetric flow-rates from the LFE and integrated hotwire measurements

Quantity	Radius 1	Radius 2
Integrated velocity profiles (m^3/s)	0.0130	0.0135
Volumetric flow-rate from LFE (m^3/s)	0.0151	
% difference from LFE value	-13.59%	-10.55%

Ideally, these two values must match in order to obey conservation of mass. However, the differences in integrated velocity profiles over the volumetric flow-rate, and the differences in velocity profiles from each other, is attributed to the random placement of pores in the test-section, which causes flow to jet through some

radial lines.

Velocity profiles were also acquired at several radial lines to serve as a base-case for comparison for the perturbation experiments. These profiles are shown in Figure 2.11. Figure 2.12 shows the velocity profiles resolved over a distance of about 1.4 hydraulic diameters from the wall [3]. It can be seen that the velocity fluctuates around the Darcy velocity because of random variations of porosity. However, the charactersitic feature of flow without perturbations is the near-wall jetting of fluid. Regardless of the circumferential location, for a distance of upto $\sim$ 4 - 7 mm (corresponding to 0.55 D_h to 1 D_h) from the wall, fluid has a tendency to ooze through, resulting in higher velocities on average in this region. Several researchers (section 1.4.4) have also observed similar flow behavior in the near-wall region. It has been observed that the porosity is higher near the walls on average, creating an alternate low-resistance path for jetting. Given the present arrangement of screens, it might be argued that the near-wall region does not have a higher porosity unlike the arrangement of spheres in a container. The screens form a snug fit against the walls of the test-section, and hence it might be reasonable to assume that the porosity is uniform all the way up to the wall for the unperturbed flow. However, if the eddies do get damped near the wall, the Forchheimer resistance is expected to be lower near the wall, since it must be remembered that the Forchheimer resistance stems from the drag force encountered due to separation behind solids and eddy shedding behind the wires of the porous medium. Having a region of lower resistance causes fluid jetting into this region. The eddy damping near the wall is explored further in Chapter 5

[3] The legends in these figures refer to several radii along which the hotwire was traversed; the significance of these radial locations will be discussed in a later section in 3.1

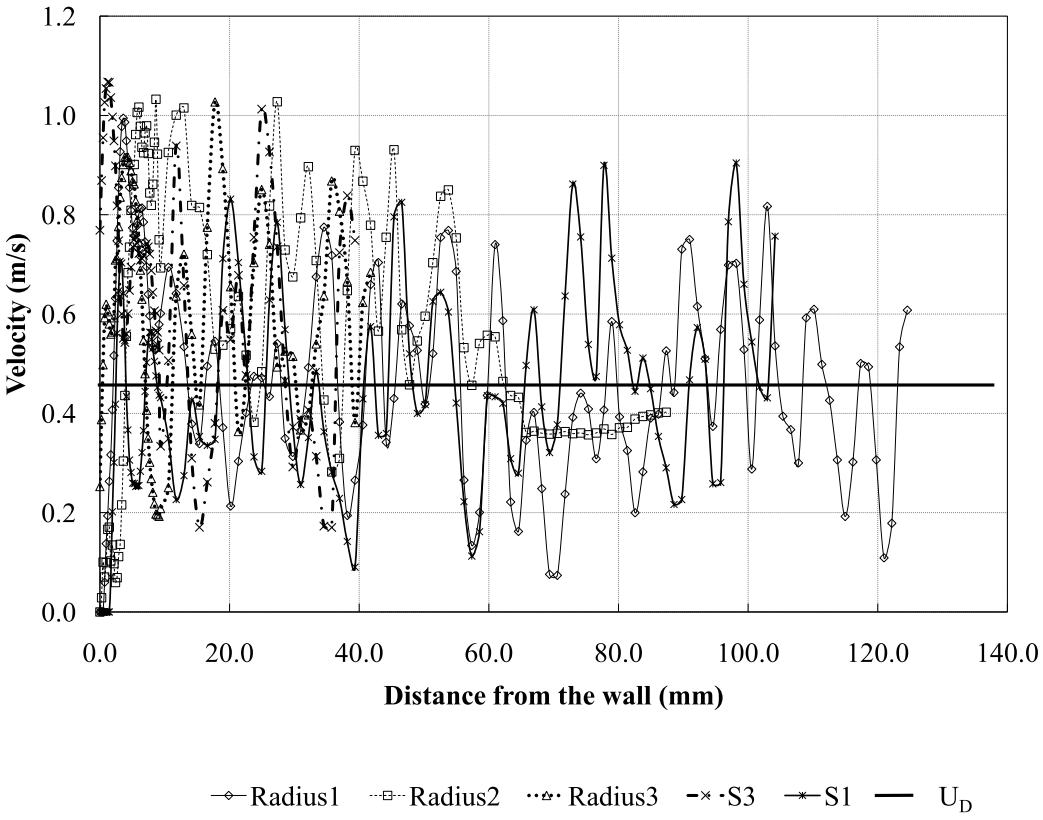

Figure 2.11: Profiles of velocity at the exit-plane of a porous medium without upstream perturbations

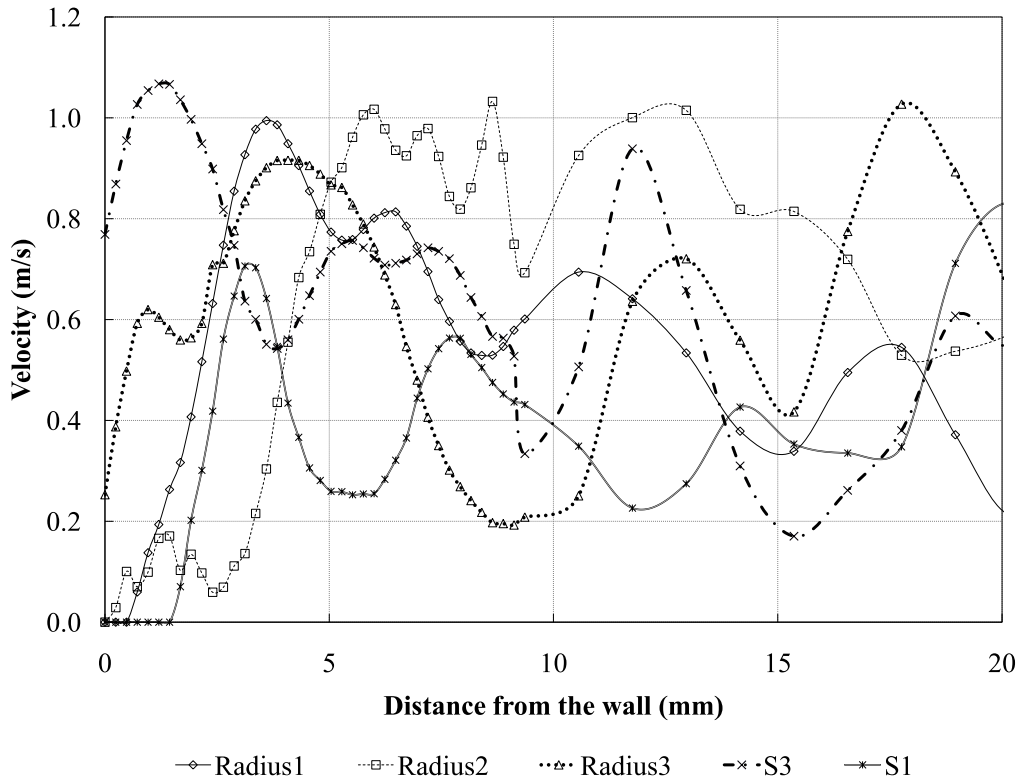

Figure 2.12: Profiles of velocity at the exit-plane of a porous medium without upstream perturbations. Near-wall region i.e. 0-10 mm from the wall, ($\sim 1.4\ D_h$) is resolved.

Chapter 3

Results: Near-wall flow perturbation experiments

3.1 Objectives

The influences of near-wall upstream disturbances on flow at the exit of the porous medium will be examined in this chapter. Profiles of velocity at the exit of the porous medium will be presented. The porous medium is fabricated as described earlier. The first one hundred screens that are used for fabricating the porous medium are of smaller diameter than the last one hundred screens, which creates an annular gap of height 4.2 mm. The annular gap acts as a bypass for flow-jetting. Four spacers that act as blockages are introduced upstream. The upstream blockage and the gap together constitute the near-wall perturbation. The flow has had an opportunity to travel twenty-one hydraulic diameters before the measurements are made. Radial traverses from the wall to about five hydraulic diameters away

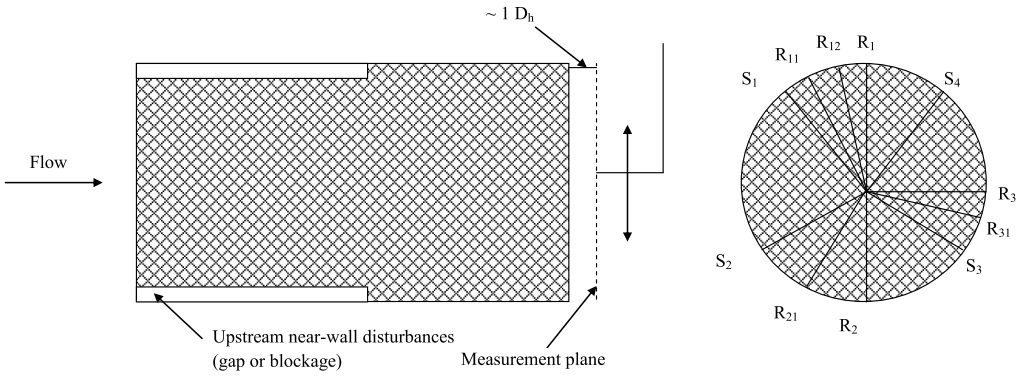

Figure 3.1: Radial locations where measurements were made

from the wall are made at several circumferential locations. Figure 3.1 is a sketch showing these circumferential locations.

To orient oneself to this figure, let us first consider the lines marked as S_1, S_2, S_3 and S_4. These indicate the locations where a spacer was placed twenty-one hydraulic diameters upstream. Radii R_1, R_2 and R_3 lie in the space between spacers, i.e. between S_1 and S_4, S_2 and S_3 and S_3 and S_4, respectively. Radii R_{11} and R_{12} lie between spacers, but not midway between spacers, i.e. in this case, between S_1 and R_1, similarly for R_{12}. Hence, the convention adopted here is that S indicates a location corresponding to an upstream spacer; R, with a single subscript, refers to a location that lies exactly in the middle of two spacers, and R with two subscripts indicates a location that is between S and R. It must be noted at this point that spacers S_1 and S_4 are placed closer to each other than 90°; in other words, the placement of upstream spacers is not axisymmetric. It must also be noted that R_1 and R_2 are diametrically opposite to each other.

By identifying the features of the flow at the measurement plane and correlating these features to the perturbations, the effect of perturbations on the flow will be studied. Also of interest is the questions concerning the radial location of the perturbation. These questions will be examined by discerning qualities of the flow from the velocity profiles.

3.2 Velocity profiles

Figures 3.2 and 3.3 present velocity profiles at radial locations corresponding to S_1, S_2, S_3 and S_4. Figure 3.3 resolves the near-wall region closely; this region is of most interest, as the disturbances to the flow placed upstream were near the wall. It can be seen from these figures that for a distance of about 3.5 mm (less than 0.5 D_h) from the wall, there is essentially no flow. Velocity profiles fluctuate about the Darcy velocity ($\sim$ 0.45 m/s) further away, after a distance of about 7 mm. The peak in velocity for S_2 at a location of around 6 mm might be attributed to a local region of high porosity, which offers a least resistance path for fluid to jet through.

Figures 3.4 and 3.5 are plots of velocity traversed at radii between the spacers, i.e. R_1, R_2 and R_3. From these figures, it can be seen that velocities near the wall (0-10 mm) at these locations are higher than those of the traverses S_1, S_2, S_3 and S_4 in Figure 3.3.

The reader is reminded that R_1 and R_2 are along a diametrical line, and, despite this, the profile looks different for these two radii. Also, the average velocity along R_1 is considerably higher than the averages of the other profiles, despite having

traversed 5 hydraulic diameters away from the wall, indicating that local regions of high porosity exist along this radial line causing local jetting.

Figures 3.6, 3.7, and 3.8 present profiles of velocity as we travel from a spacer to the space between spacers circumferentially. The near-wall region is resolved to focus our attention on the flow features in that region.

From these figures, it can be seen that the radial traverses that correspond to upstream spacers have the lowest velocity (as seen by profiles S_1, S_2 and S_3), and the profiles that are located in the middle of two spacers have the highest velocity (as seen by profiles R_1, R_2 and R_3) The remaining profiles fall between these two extremes.

In order to examine the effect of an upstream perturbation, the profiles acquired at the radial locations shown in Figure 3.1 are compared to profiles acquired for the unperturbed case at the same radial locations, with flow through the porous medium without upstream blockages or gaps. It must be noted at this point that only the near-wall flow is of significance here. Also it must be noted that the screens constituting the porous medium were restacked for the two experiments and hence the pore-distribution in the core-flow (region away from the walls) might be somewhat different. From earlier presentation of results for the unperturbed case, it was observed that the near-wall flow features did not change from one radial line to another, and hence for the unperturbed case, any radial line is representative of the flow. In the following discussion, the radial lines for the unperturbed case are isolated only for the sake of facilitating easier comparison to profiles acquired for the cases with upstream perturbations.

Figure 3.9 highlights the difference in near-wall flow for the unperturbed and perturbed case along the radius R_1. The presence of an upstream gap has accelerated the flow further from what was observed for the unperturbed case. Similar features can also be discerned from velocity profiles for the unperturbed and perturbed cases obtained at radial line R_3, shown in Figure 3.10, although the difference in near-wall flow features between the two profiles is not as marked as it is for R_1.

Perhaps the most striking difference in flow features can be observed from Figures 3.11 and 3.12, which shows velocity profiles obtained at radial lines S_1 and S_4, for the unperturbed and perturbed cases. These radial lines for the perturbed cases correspond to an upstream blockage, and it was shown in earlier figures that the blockage resulted in a near wall-deficit that persisted all the way to the exit plane, despite twenty-one hydraulic diameters of travel in the streamwise distance. This feature of the perturbed flow is highlighted in Figures 3.11 and 3.12 by comparing the velocity profiles to those for the unperturbed cases.

Flow through a porous medium without any perturbations is characterized by near wall jetting of flow, as seen by the slight excess in velocity for about 4 mm away from the wall ($\sim$ 0.5 D_h). An upstream perturbation, such as a gap or blockage distorts this feature, and either facilitating acceleration of flow toward this near-wall region (in the case of the gap) or diversion of flow away from the near-wall region (in the case of a blockage). What remains rather unbelievable is that the distortion of flow features are not erased after the flow has traveled twenty-one hydraulic diameters in the streamwise direction, and remnants of flow distortion exist in the flow exiting from the porous medium.

3.3 Integrated velocity profiles

As discussed earlier in section 2.2, jets and wakes that are present as a result of a upstream gaps or blockages lead to an excess or deficit flow through an area that scales on the size of the gaps or blockages respectively. This was also witnessed in the velocity profiles shown in Figures 3.2 to 3.12. To quantify this excess or deficit flow, the velocity profiles obtained at the radial locations shown in Figure 3.1 are integrated over a radial distance of one hydraulic diameter from the wall:

$$Q_{nw} = \int_0^{D_h} 2\pi r U dr \tag{3.1}$$

This distance is chosen arbitrarily, but is chosen so that it is of the same order of magnitude as the gap or blockage (whose characteristic size is $\sim 0.5\ D_h$). Tables 3.1 and 3.2 show these integral quantities obtained at radial lines corresponding to upstream blockages and upstream gaps respectively. The values of Q_{nw} are normalized on the volumetric flow-rate through the test-section, Q, and is shown in these tables. The normalized flow rate is an indication of fraction of the total flow in the near-wall region. However, it should be noted that a distance of 1 D_h corresponds to about 0.5 % of the total cross-sectional area, and hence, only a small fraction of the total flows through this area. The values of Q_{nw} normalized on Q are expected to be small.

Table 3.1: Integrated velocity profiles over 1 D_h for radial lines S_1, S_2, S_3, S_4

Radial lines	Q_{nw} x $10^{-5} m^3/s$	Q_{nw} x 100/Q
S_1	1.87	0.12
S_2	8.66	0.57
S_3	5.53	0.37
S_4	6.55	0.43

It can be seen from Tables 3.1 and 3.2 that the integrated velocity over a distance of 1 D_h for profiles with upstream gaps is nearly twice that for profiles with upstream blockages, indicating excess flow in radial lines corresponding to upstream gaps.

Table 3.2: Integrated velocity profiles over 1 D_h for radial lines R_1, R_2, and R_3

Radial lines	Q_{nw} x $10^{-5} m^3/s$	Q_{nw} x 100/Q
R_1	13.2	0.87
R_2	12.7	0.84
R_3	13.2	0.87

Perhaps a useful quantity is the difference between the integrated velocity for the perturbed flow over the integrated velocity (integrated over the same area as the perturbed flow) for unperturbed flow, Q_{nwu}.

$$Q_D = \frac{Q_{nw}}{Q_{nwu}} - 1 \tag{3.2}$$

It must be noted here that Q_{nwu} was obtained by integrating velocity profiles for the unperturbed flow shown in 2.11 over a distance of 1 D_h from the wall. The values of Q_D are listed in Table 3.3.

Table 3.3: Difference in integrated velocity profiles between unperturbed and perturbed flows

Radial lines	$Q_D = \frac{Q_{nw}}{Q_{nwu}} - 1$
R_1	0.0013
R_3	0.06
S_1	-0.71
S_4	-0.48

It can be seen from Table 3.3 that when the flow passes through an upstream gap, the integrated velocity is nearly equal to that of the flow without any upstream perturbations, and isolating the effect of an upstream gap in the near-wall region is rendered somewhat difficult. Although this might raise the question whether upstream perturbations have any effect at all on the flow, the large negative values of Q_D for flow with upstream blockages (corresponding to integrated profiles along lines S_1 and S_4) indicate distortion of the near-wall flow as a result of upstream perturbations. The deficit in near-wall flow at these radial lines indicate that the flow has avoided passing through upstream blockages, and is prevented from redistributing itself despite traveling through twenty-one hydraulic diameters.

3.4 Summary of near-wall perturbation experiments

The measurements shown in this chapter addresses some questions that were raised earlier concerning the nature of the flow with upstream perturbations. The first conclusion that one draws from these measurements is that there is no representative velocity profile because of near-wall jets and deficits in velocity. Farther away from the wall, local regions of high and low porosity prevent velocity profiles from being "representative" of the porous medium. This causes considerable difficulty in drawing meaningful conclusions from a single velocity profile, acquired along a radial line. Several radial traverses must be acquired to characterize the flow features.

It is also evident that upstream near-wall perturbations affect flow features despite traveling nearly twenty-one hydraulic diameters in the streamwise direction within the porous medium. One might have thought that this distance would have allowed plenty of opportunity for redistribution. When flow enters the porous medium, it sees blockages caused by spacers and rushes circumferentially to the space between spacers (the annular gaps near the wall offer a path of low-resistance). This causes much of the fluid to jet through the space between blockages. This jet preserves itself all the way until the exit of the porous medium.

Random variations in porosity exist in the porous medium making the signal to noise ratio of measurements lower, and making the identification of coherent features difficult. The general trend that can be observed is that near-wall, upstream wakes and jets generated by blockages and gaps, respectively, persist far

downstream. Figures 3.7 to 3.8 offer some distinction of flow features as we move circumferentially, showing that flow features in the near-wall region are not identical for all radii.

Along the same diameter, there seem to be variation in profiles (i.e. R_1 and R_2) which are attributed to two effects. The placement of upstream spacers is not uniform, i.e. the geometry is non-axisymmetric; R_1 lies between two spacers, S_1 and S_4, that are placed closer together than two spacers between which the location R_2 lies. Flow accelerates in a smaller region when the spacers are closer and a higher velocity is attained; hence, velocities measured along R_1 are higher than those along R_2, although they lie along the same diameter. Further away from the wall as we travel along R_1, there appears to be a region of high porosity, causing further jetting. This region of high porosity is an artifact of the porous medium fabrication.

The reason for persistence of upstream perturbations and poor redistribution of the flow has not been investigated in the literature so far. The porous media literature survey presented earlier hints that eddies shed within the porous medium are damped near the wall. It was also suggested that this damping is as a result of porosity variation. These eddies are responsible for transport enhancement in porous media, and the fact that they are suppressed by the wall might reduce radial transport near the wall. Hence, redistribution and spreading rates of jets and wakes are reduced, preserving them to the exit plane. If, indeed, poor transport as a result of near-wall suppression of eddies is the culprit for the persistence of flow features presented here, verifying this hypothesis would require placement of a jet or a wake far away from the wall and within the porous medium, and observing the characteristics of such a flow.

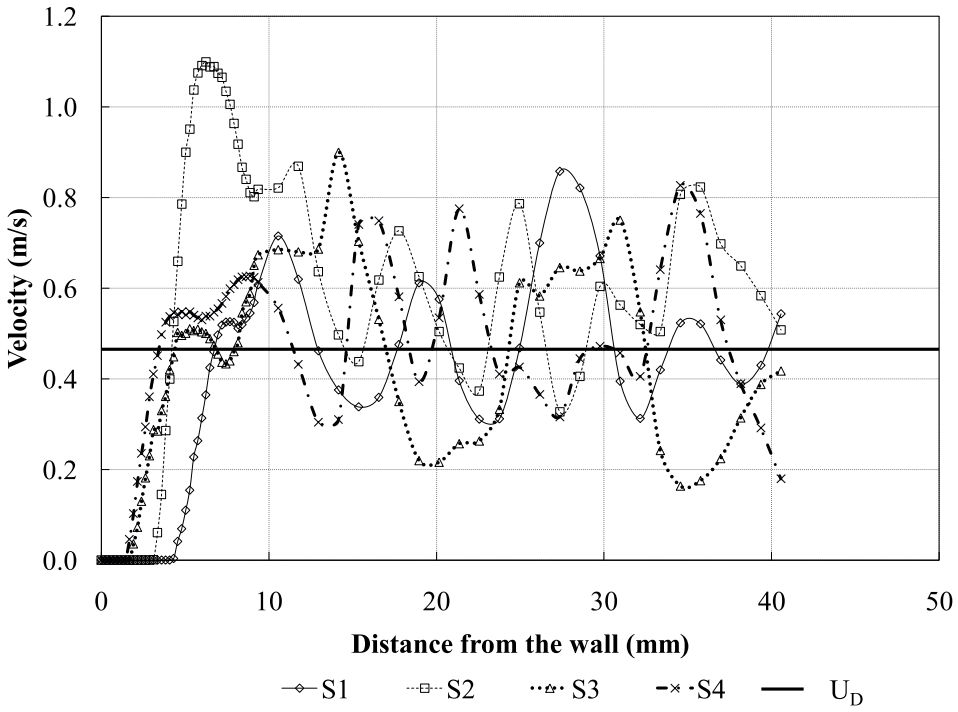

Figure 3.2: Velocity profiles at radii S_1, S_2, S_3 and S_4 at the measurement plane.

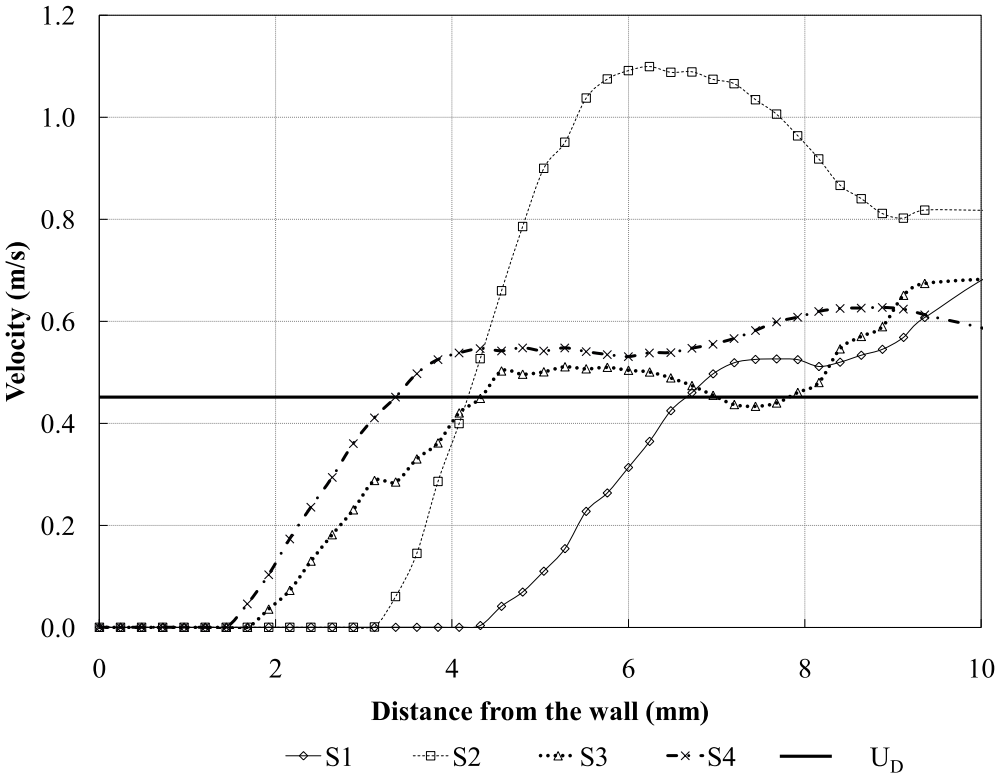

Figure 3.3: Velocity profiles at radii S_1, S_2, S_3 and S_4 at the measurement plane. Near-wall region (0-10 mm, i.e. $\sim 1.5\ D_h$) is resolved

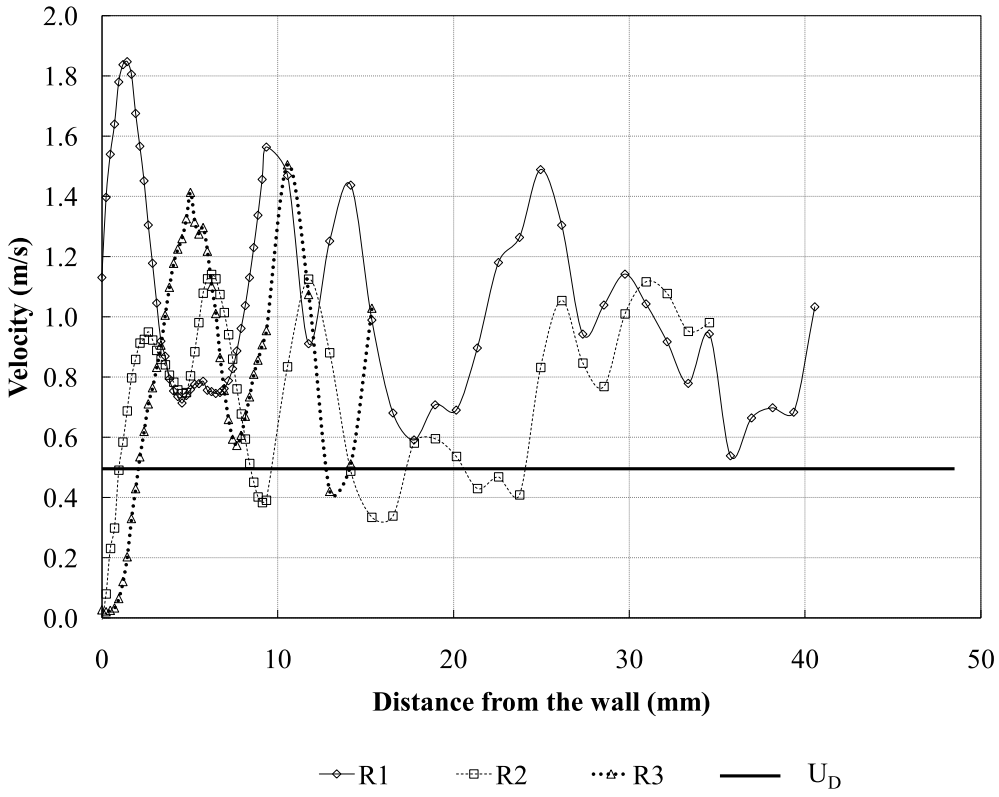

Figure 3.4: Velocity profiles at radii R_1,R_2, and R_3 at the measurement plane.

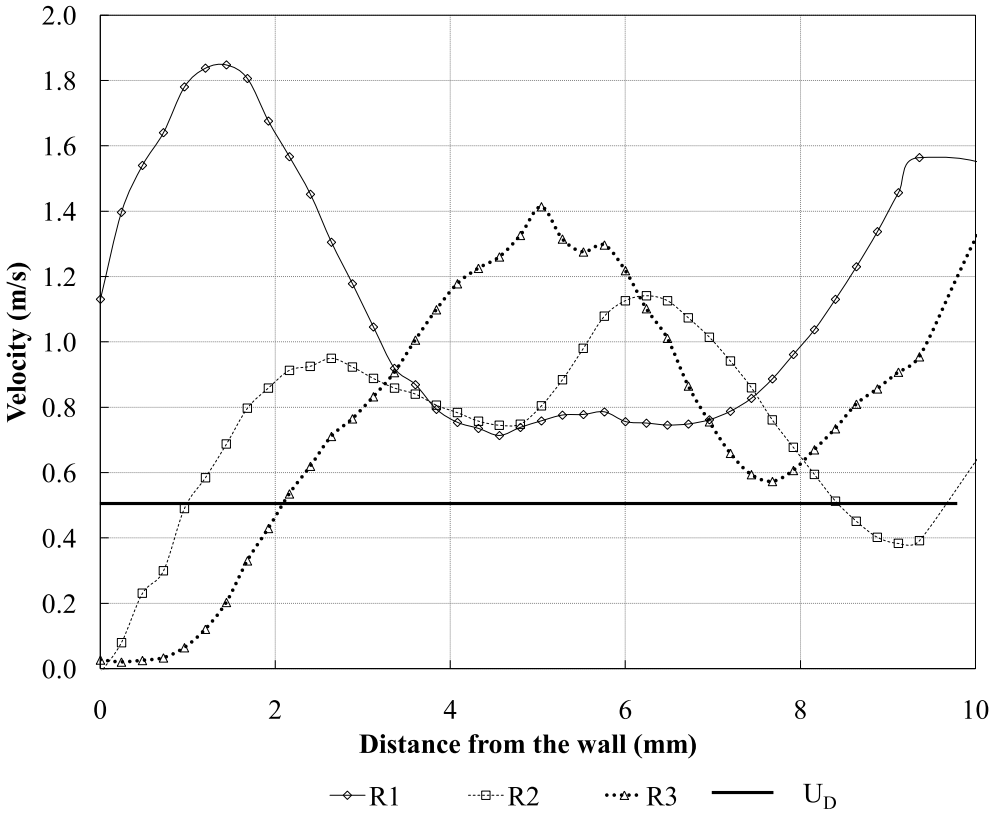

Figure 3.5: Velocity profiles at radii R_1,R_2, and R_3 at the measurement plane. Near-wall region (0-10 mm, i.e. $\sim 1.5\ D_h$) is resolved

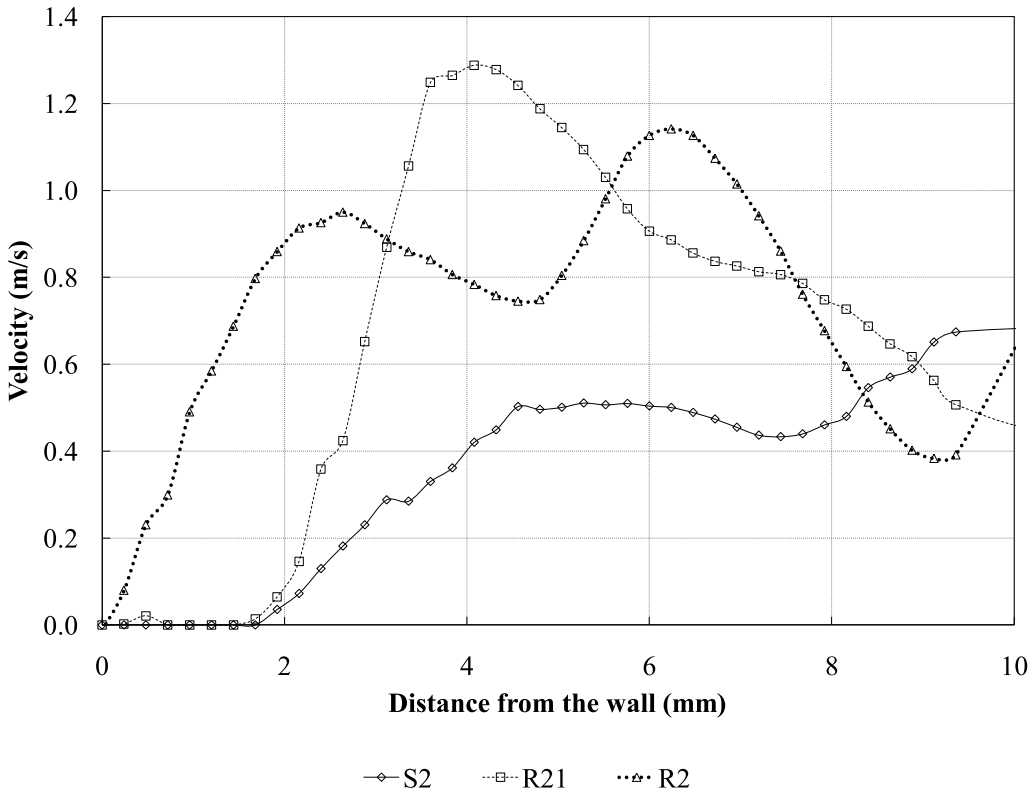

Figure 3.6: Velocity profiles at S_2, R_{21}, and R_2 at the measurement plane. Near-wall region (0-10 mm, i.e. $\sim 1.5\ D_h$) is resolved

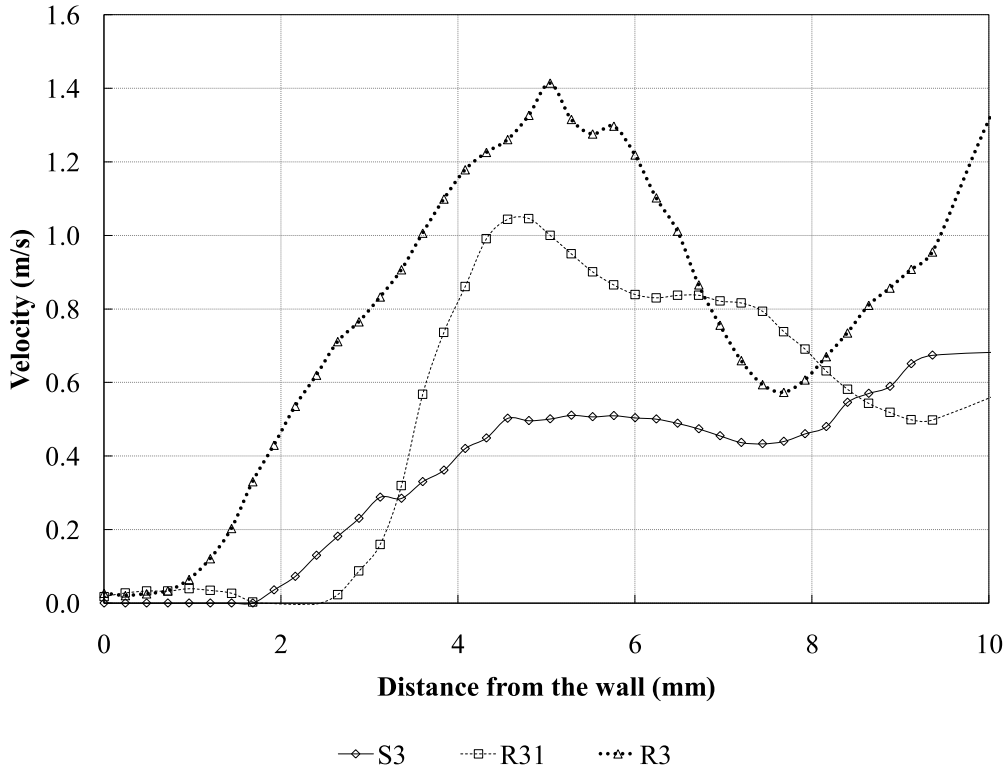

Figure 3.7: Velocity profiles at S_3, R_{31}, and R_3 at the measurement plane. Near-wall region (0-10 mm, i.e. $\sim 1.5\ D_h$) is resolved

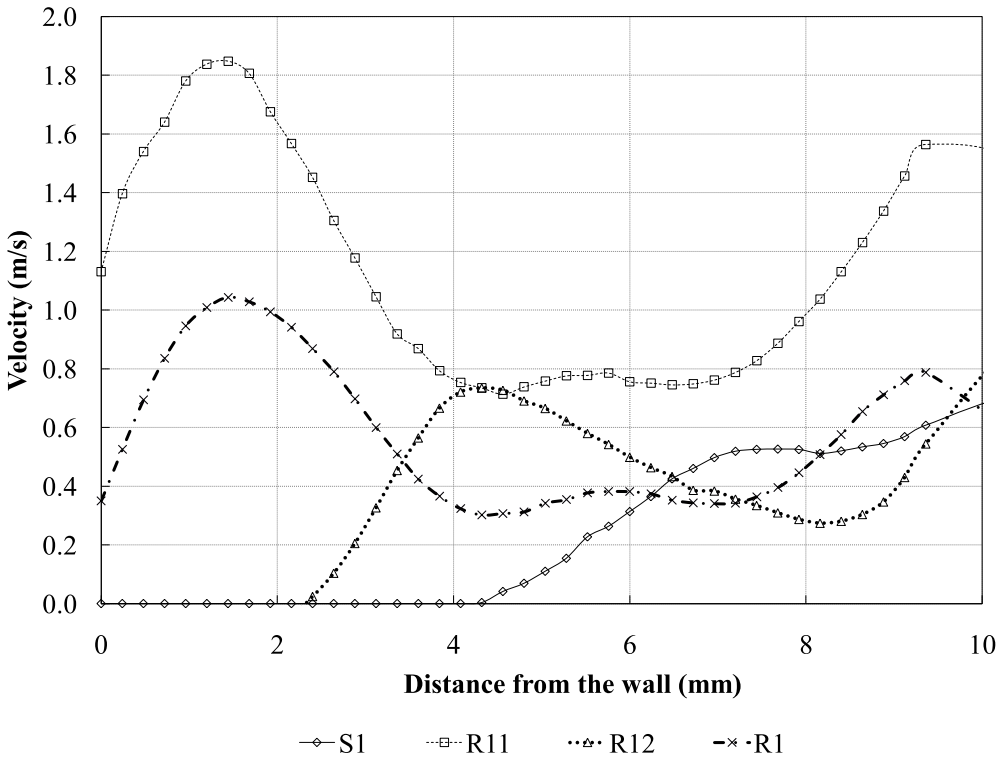

Figure 3.8: Velocity profiles at S_1, R_{11}, R_{12}, and R_1 at the measurement plane. Near-wall region (0-10 mm, i.e. $\sim 1.5\ D_h$) is resolved

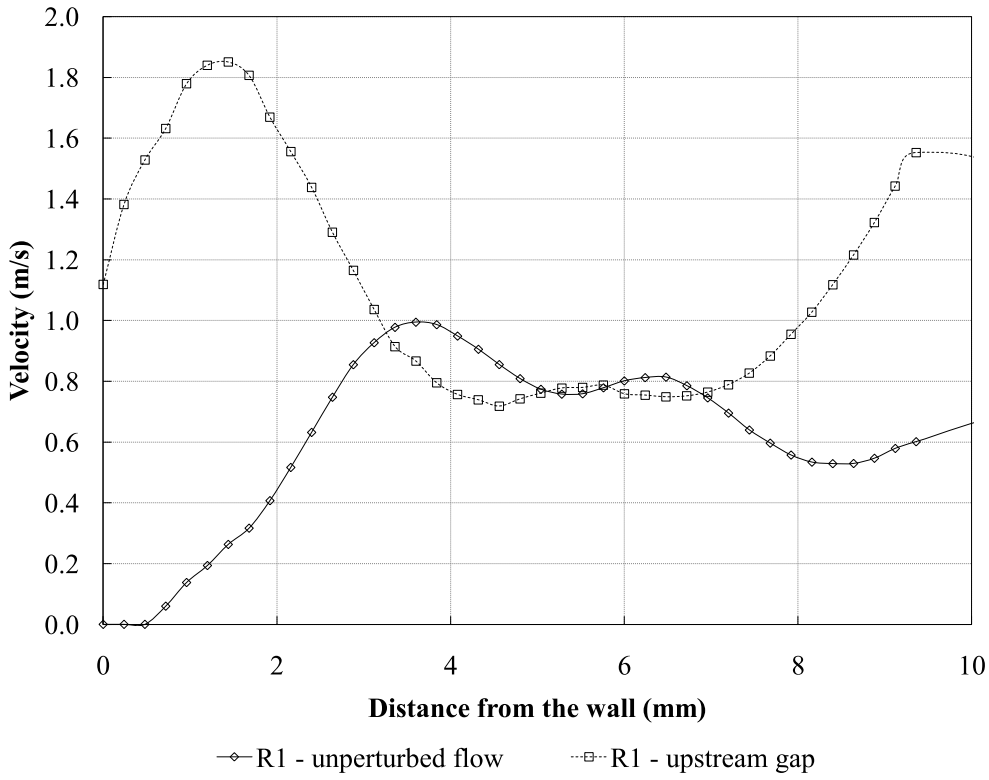

Figure 3.9: Velocity profiles at R_1 at the measurement plane for the unperturbed flow and with an upstream gap. Near-wall region (0-10 mm, i.e. $\sim 1.5\ D_h$) is resolved

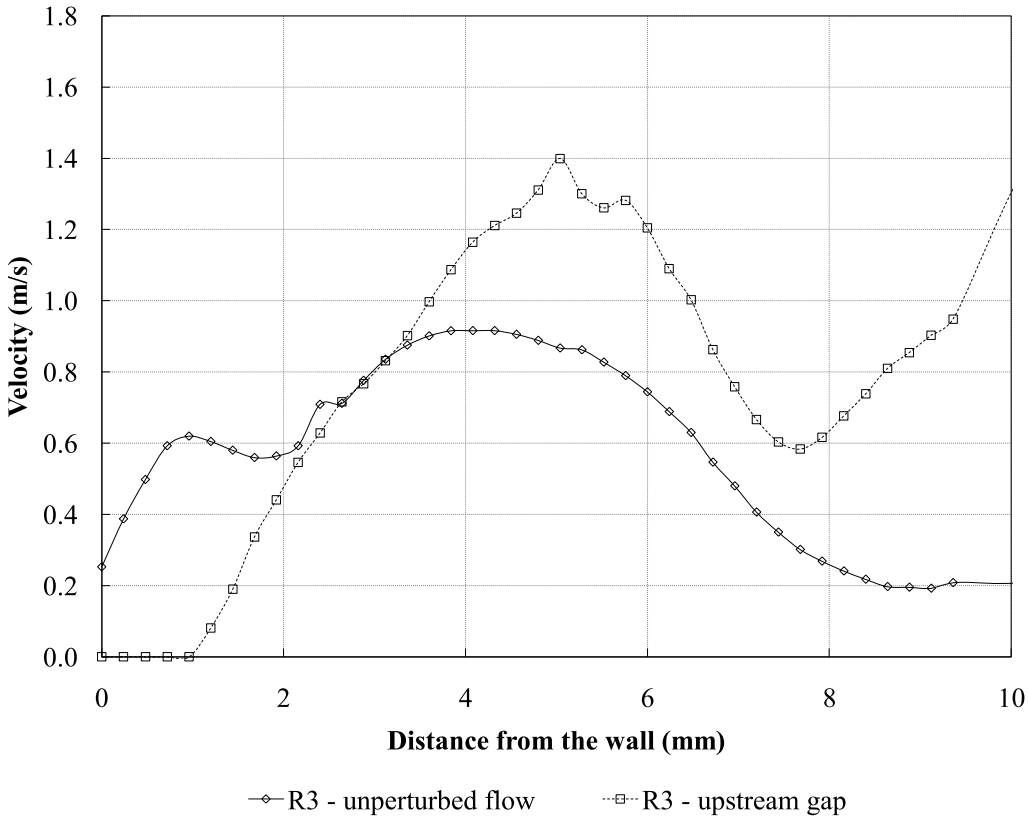

Figure 3.10: Velocity profiles at R_3 at the measurement plane for the unperturbed flow and with an upstream gap. Near-wall region (0-10 mm, i.e. $\sim 1.5\ D_h$) is resolved

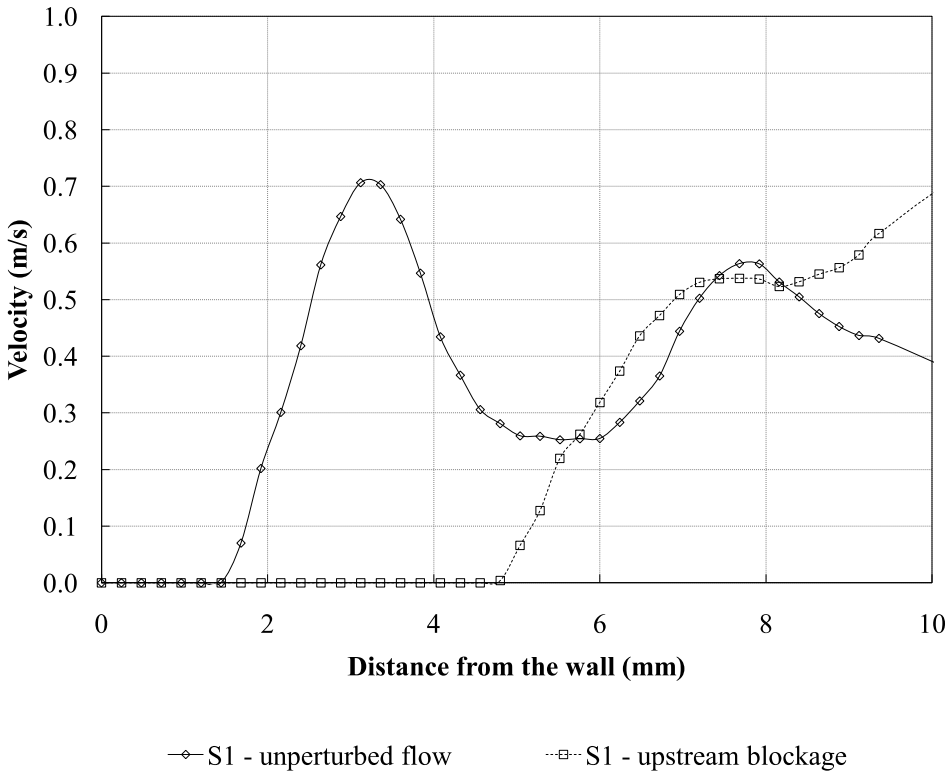

Figure 3.11: Velocity profiles at S_1 at the measurement plane for the unperturbed flow and with an upstream gap. Near-wall region (0-10 mm, i.e. $\sim 1.5\ D_h$) is resolved

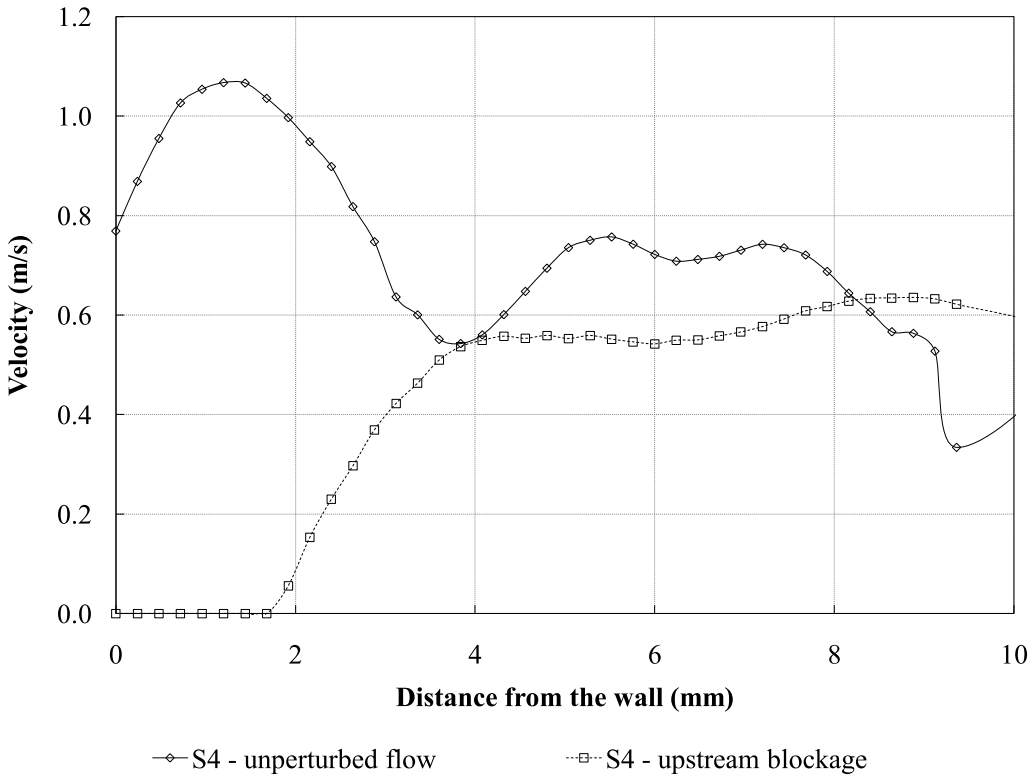

Figure 3.12: Velocity profiles at S_4 at the measurement plane for the unperturbed flow and with an upstream blockage. Near-wall region (0-10 mm, i.e. $\sim 1.5\ D_h$) is resolved

Chapter 4

Results: Core-flow perturbation experiments

4.1 Objectives

Experiments were conducted to verify the hypothesis that though poor redistribution of flow occurs near the wall due to pore-scale eddies being damped, redistribution is effective in the core where the eddies are not damped. These experiments involved placing upstream disturbances in the "core" of the porous matrix, i.e. farther away from the walls of the container containing the screens. Figure 4.1 shows a sketch of these disturbances. The perturbations were either holes cut through 100 screens (a bypass) or paper discs placed on those 100 screens (a blockage); the diameter of the hole and the paper disc was ~ 1 cm ($1.4\ D_h$); the hole or disc diameter is of the same order as the near-wall perturbations discussed earlier (in section 3.1). The results of the core-flow disturbance experiments are

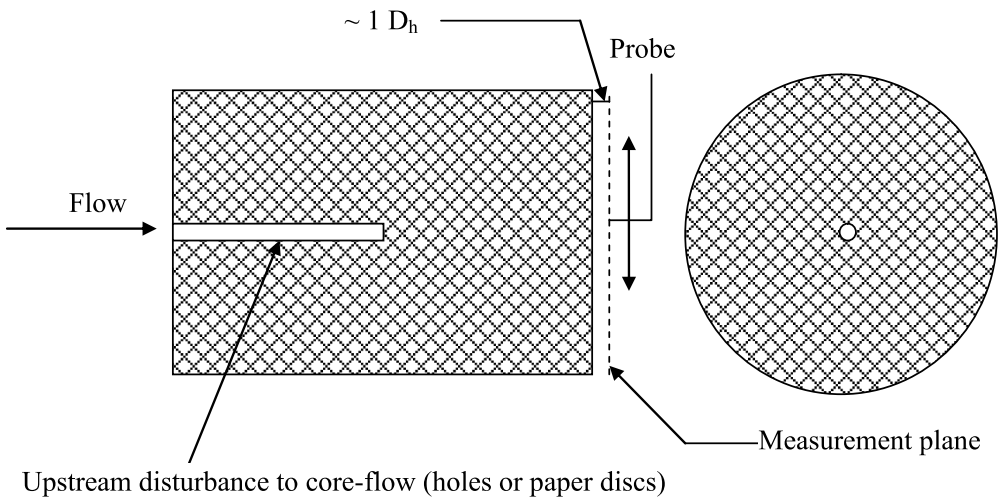

Figure 4.1: Upstream disturbances to core-flow

presented in this chapter.

4.2 Jet spreading through the core of the porous medium

Velocity measurements were taken using a hotwire as flow exits the porous medium. Upstream disturbances to the core-flow were offered by a hole of diameter 1 cm at the center of the screens. One-hundred such screens with holes in the center were stacked upstream, allowing flow to jet through. Flow is then allowed to pass through 100 downstream layers of screen without holes in them; this distance corresponds to twenty-one hydraulic diameters of travel in the streamwise direction to allow redistribution and spreading of the upstream jet. Figure 4.2 shows these

velocity profiles. The hotwire was traversed radially outward on either side, for a distance of 25 mm ($\sim$ 4 D_h) from the center on the measurement plane. Three different radial profiles were considered, and these are denoted as J_1, J_2, and J_3 in Figure 4.2.

From Figure 4.2, the first discerning and obvious feature of this flow is that it is nearly axisymmetric, and there is not much of a variation in the velocity profiles at variour radii. Figure 4.3 isolates one of these radial profiles, J_1, as a "representative" radius to study the features of this flow. A distance of 10 mm (1.4 D_h) on either side of the center of the measurement plane is resolved. Recall that the diameter of the upstream hole was 1 cm, and a jet, if it exists, would grow in the matrix beginning with the size of the hole.

The velocity profile shown in Figure 4.3 indicates that flow has redistributed after streamwise travel through the porous medium lasting twenty-one hydraulic diameters. No evidence of the jet that streaked through the low-resistance passage offered by the upstream holes exists. The velocity at each point in the profile wiggles about the Darcy velocity ($\sim$ 0.45 m/s), as a result of distributed regions of low and high porosity in the random wire porous matrix. The characteristics of this flow are similar to those observed for unperturbed flow through the porous medium (Section 2.6 and figure 2.11) .

4.3 Wake spreading through the core of the porous medium

Velocity measurements were taken as the flow exits the porous medium at the measurement locations. Upstream blockages placed in the core region of the porous matrix were offered by paper discs of diameter 1 cm which were placed at the center of the screen; 100 such screens, followed by 100 screens without any perturbation to the flow were used, again corresponding to twenty-one hydraulic diameters of downstream travel, giving an opportunity for flow to avoid the upstream blockage, and a wake in the core-flow to evolve.

Figure 4.4 shows these velocity profiles for three radial traverses of the hotwire, indicated by W_1, W_2 and W_3, extending to a radial distance of 25 mm ($\sim 4\ D_h$) on either side from the center of the measurement plane.

Isolating one of these radial profiles as a "representative" profile, as there is no discernible difference between the radial profiles, and resolving a radial distance of 10 mm (1.4 D_h) on either side of the center, Figure 4.5 shows that features of this flow are similar to what was seen for the previous case with the upstream hole: no evidences of a wake exists, and velocity fluctuates about the Darcy velocity of 0.45 m/s.

It must be noted that only the upstream 100 screens were restacked, and the downstream 100 screens were left undisturbed from the arrangement of the experimental case with a hole placed in the upstream portion of the core of the porous medium. The velocity profiles for these two sets of experiments are plotted together in Figure 4.6.

It can be seen that these profiles nearly align, indicating that regardless of the nature of the upstream disturbance to core-flow, the disturbance has been erased by the flow. Thus, flow features at the measurement plane are dictated by topology of the porous medium in the last few hydraulic diameters upstream of the measurement plane. An upstream jet and an upstream wake are both erased if the perturbation causing the jet or the wake is placed in the core-flow.

Setting the results of these experiments against the results of the near-wall perturbation experiments, the differences are obvious: in the case of a near-wall perturbation, distortions to the flow caused by the perturbation are not distributed despite the flow traveling a streamwise distance of twenty-one hydraulic diameters. If a blockage is placed near a wall, a wake develops which is preserved all the way to the measurement plane at the exit of the porous medium; a near-wall gap causes flow jetting, which is also preserved all the way to the exit of the porous medium. A blockage or a hole placed away from the wall in the core-flow causes disturbance to the flow which is redistributed as a result of streamwise travel, and features of the flow are similar to those for unperturbed flow through the porous medium. The spreading rate of the upstream jet and the upstream wake are perhaps similar, and the velocity profiles obtained for the two cases align as long as the flow travels through a porous medium of similar topology in the downstream section of streamwise travel.

The earlier hypothesis about suppression of pore-scale eddies by walls, and concomitant poor redistribution of flow in the near-wall region is supported by the core-flow experiments. The near-wall and core-flow experiments suggest that strength of redistribution of flow is vastly different in the two regions of the flow.

This also suggests that radial transport is inefficient near the walls, in comparison to transport in the core-flow; axial transport is perhaps better in comparison to radial transport near the walls as there is no damping of eddies in the axial (streamwise) direction, possibly rendering the flow anisotropic, a fact to be remembered when employing porous media for heat transfer and thermal storage.

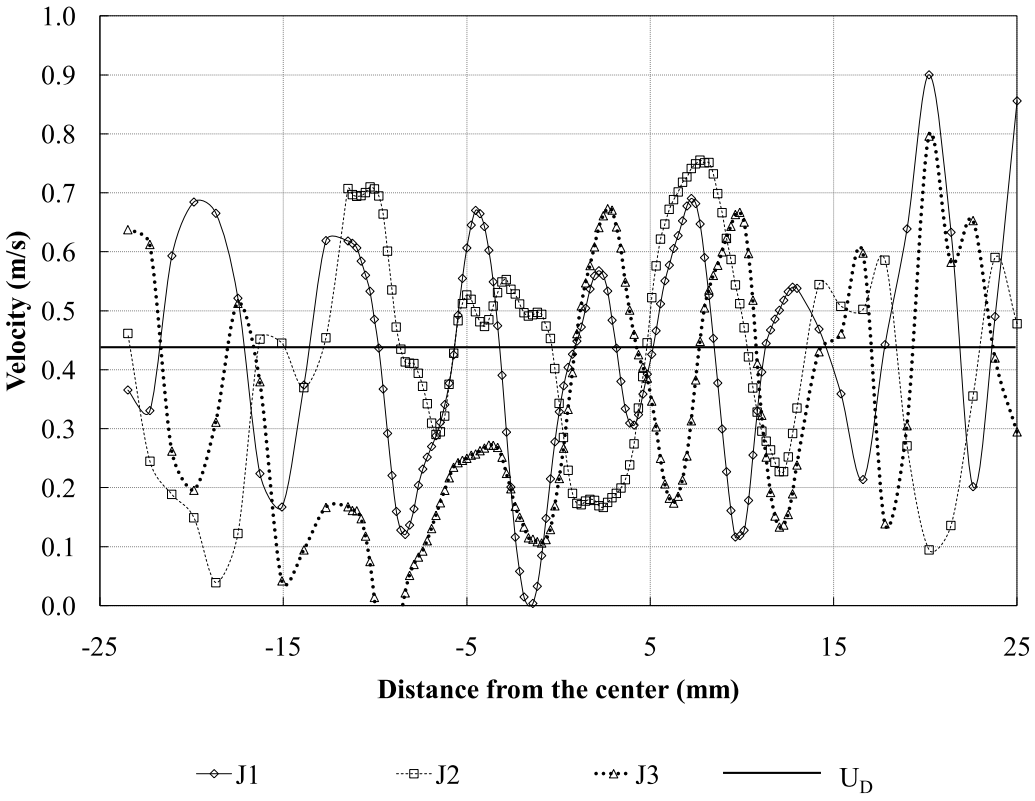

Figure 4.2: Velocity profiles at the measurement plane with upstream holes to perturb the core-flow

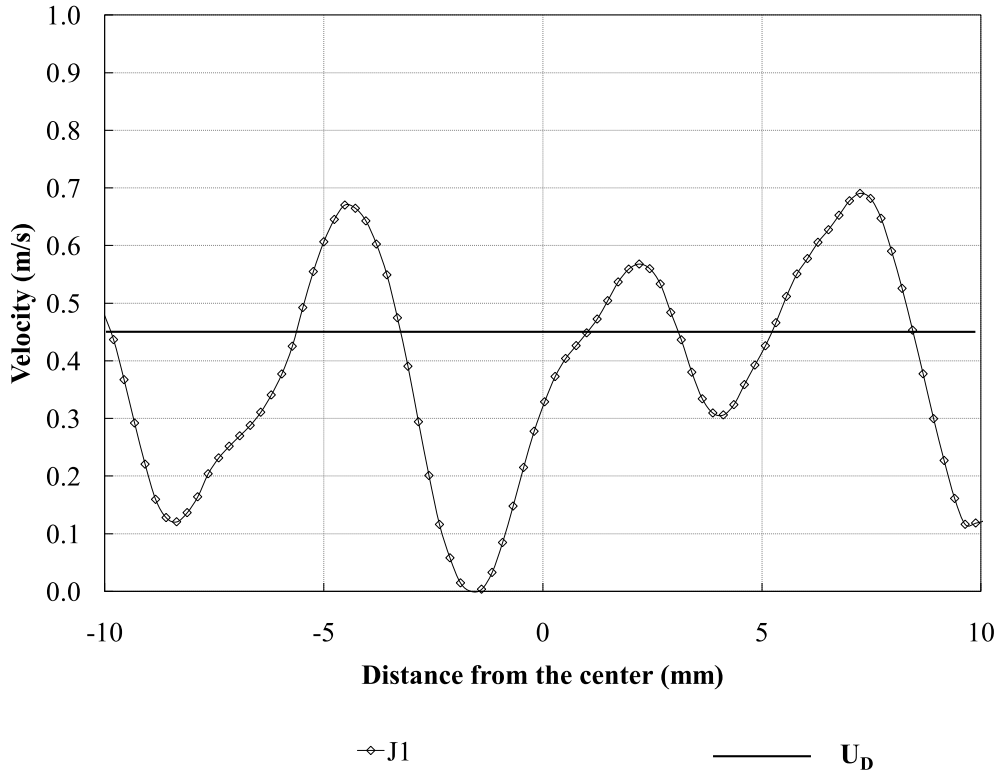

Figure 4.3: Velocity profiles at the of the porous medium with upstream holes to perturb the core-flow (0-10 mm from the center $\sim 1.4\ D_h$ resolved on either side)

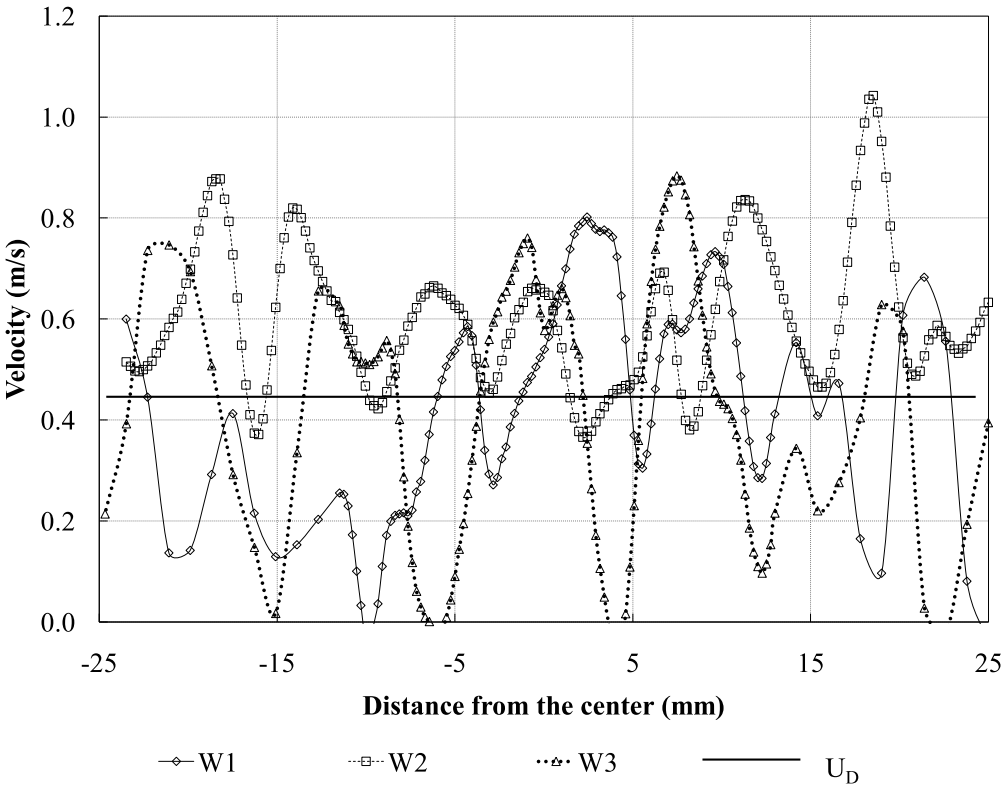

Figure 4.4: Velocity profiles at the measurement plane with upstream blockages to perturb the core-flow

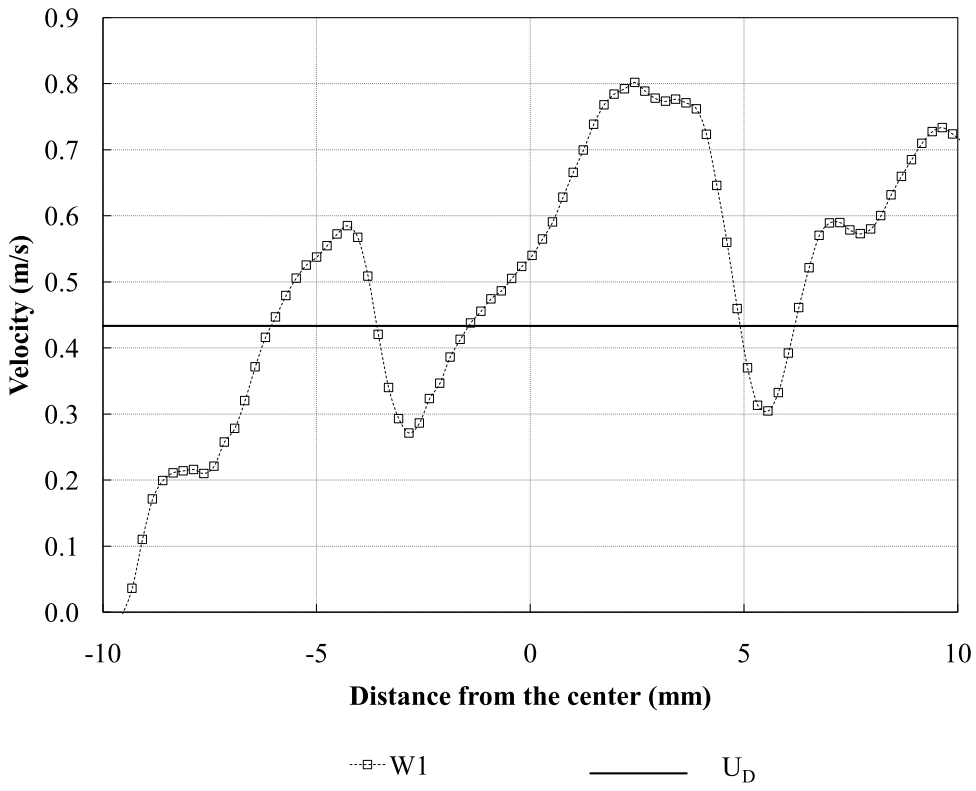

Figure 4.5: Velocity profiles at the measurement plane with upstream blockages to perturb the core-flow (0-10 mm from the center $\sim$ 1.4 D_h resolved on either side)

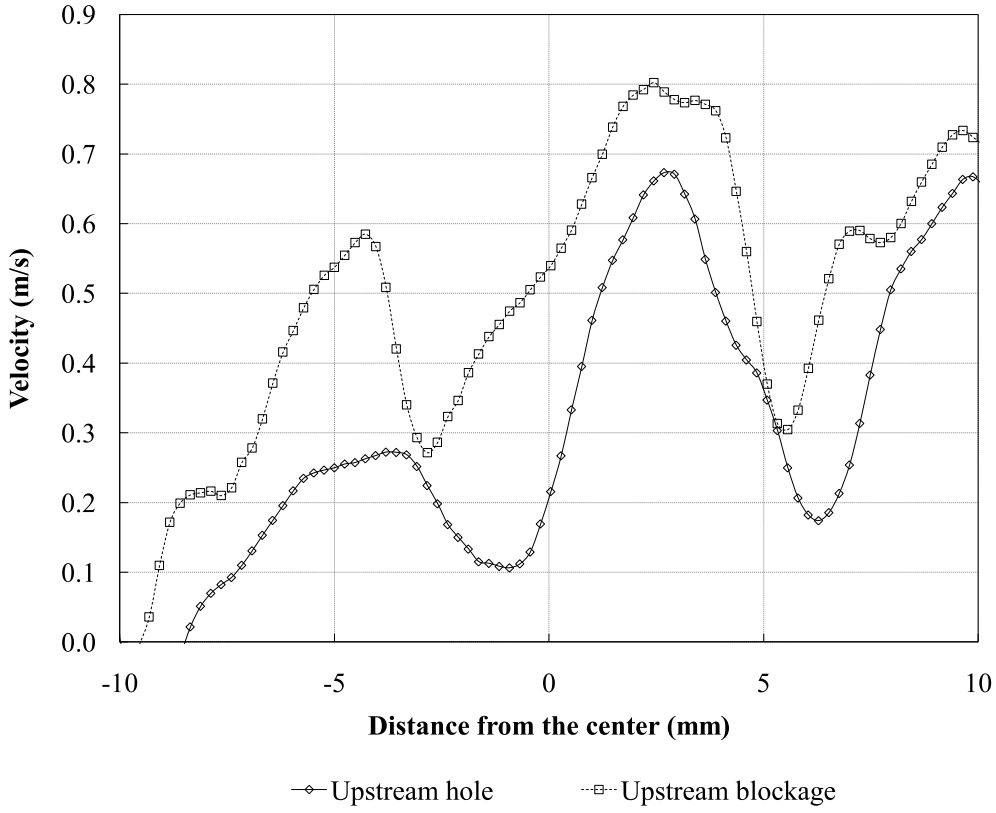

Figure 4.6: Comparison of velocity profiles with upstream holes and blockages to perturb the core-flow (0-10mm from the center $\sim$ 1.4 D_h resolved on either side)

Chapter 5

Pore-scale eddy transport in porous media

Experiments on porous media flows considered in Chapters 3 and 4 show that upstream jets and wakes tend to preserve themselves in the near-wall region and evidences of upstream jets and wakes are not erased as a result of streamwise travel through the porous medium. Upstream jets and wakes in the core-flow away from the wall of the porous matrix, however, redistribute as a result of mixing within the porous medium. It is suspected that the strength of mixing caused by pore scale eddy transport was stronger in the core of the porous medium and weaker in the near-wall region, enabling better transport in the core flow, causing jets and wakes to redistribute themselves. In this chapter, the strength of eddy transport in near-wall region and in the core are examined. It must be kept in mind that no direct measurements of eddy transport in different regions of the flow have been performed in the present study, and the characteristics of eddy transport are

inferred from previous work on pore scale eddies in the near-wall and in the core of the matrix. The objective of this chapter is merely to show by means that are not rigorous, how eddy transport varies in different regions of the flow.

The eddy component of dispersion arises from pore scale eddies. The mechanism for the generation of pore scale eddies is different from that of turbulent eddies. Nonetheless, based on evidences seen in porous media flows, eddies shed within pores from the solid obstructions show similar behavior to those of turbulent eddies. (For instance, see Hall and Hiatt (1996) and Seguin et al. (1998)). It might then be possible to model eddy component of dispersion in porous media using methods that have been employed for studying turbulent flows.

Prandtl's mixing length hypothesis is a classic model that has been employed for characterizing eddy transport in free turbulent flows. Niu (2005) extended this model (section 1.4.3) which proposes from dimensional arguments that the eddy transport in turbulent flows can be cast in terms of a charactersistic length scale of the eddy, l, and characteristic eddy velocity U, as:

$$\epsilon_M = \Lambda l U \tag{5.1}$$

where Λ is a constant sometimes referred to as diffusivity coefficient. It has been suggested by Niu that this model can be applied to compute eddy component of dispersion of the pore scale eddies using the average pore diameter (hydraulic diameter), D_h as the length scale of eddies and the Darcy velocity as the characteristic eddy velocity.

Direct measurements of fluctuating components of velocity enabled the estimation

of eddy component of dispersion for a high porosity porous matrix under steady flow conditions. It was proposed that the eddy component of dispersion for similar porous matrices was:

$$\epsilon_M = 0.02 U_D D_h \tag{5.2}$$

Niu's measurements were performed in the core of the porous matrix, where the velocity of the eddies can be assumed as the Darcy velocity and the hydraulic diameter (or average pore-size) is representative of the eddy size. In other words, the eddies are of constant size (and are, on average, the size of the pore) and the they are convected with the Darcy velocity. It might be reasonable to assume that in the core of the porous matrix in the present study, the eddy component of dispersion can be described by this model. In the near-wall region, however, this model breaks down since it is not reasonable to expect that the eddies do not shrink in size as they approach the wall.

As examined in section 1.4.4, some researchers have used simple damping models for packed beds of low porosity using an exponential decay or a linear damping of the eddy component of dispersion. The justification provided by researchers for employing such models is that the porosity of the packed beds shows an exponential decay in the near-wall region. In the present study, the porosity variation near the wall is unknown because of the random stacking of screens. In the case of near-wall perturbations placed upstream, such as in the gap, the porosity of the gap (100 %) is higher than that of the core of the matrix (90 %). In the case of the near-wall blockage, the porosity (0 %) is lower than that of the matrix. Hence, there is a step change in porosity in the region where the perturbation

is placed. Downstream of the perturbation in the near-wall region, the porosity variation is unknown, but it can be assumed to be small because of the snug fit of the screens against walls of the test-section. Hence, coupling the eddy damping in the near-wall region to porosity variation lacks physical intuition for the present arrangement of pores in the porous matrix, and the approach followed by packed bed research is not suitable for the present case.

In this context, near-wall flows in free (unobstructed turbulent boundary layers) is examined under the assumption that high-porosity porous media flows are likely to be similar to unobstructed turbulent flow than flow through packed beds. Hall and Hiatt (1996) for instance, show decay of velocity fluctuations which follow a $-5/7$ power law, which is observed for isotropic turbulence generated from grids. (Roach (1987)) Similar turbulent-like behavior has also been reported based on spectral measurements inside a porous medium taken by Masuoka and Takatsu (2002).

Prandtl's mixing length model has been extended to the near-wall region of unobstructed turbulent flows (Schlichting et al. (2000)). These are based on the assumption that the eddies tend to shrink in size and transport very near the wall is achieved at molecular scales. In the near-wall region of unobstructed turbulent flows, it has been suggested that the mixing length or the charactersitic size of the eddy, l, is:

$$l = \kappa y \qquad 0 < y \leq \frac{\lambda\delta}{\kappa} \tag{5.3}$$

$$l = \lambda\delta \qquad \frac{\lambda\delta}{\kappa} \leq y \leq \delta \tag{5.4}$$

Here, y is the distance from the wall and λ and κ are constants of the model (taking values 0.09 and 0.41 respectively).

Equations (5.3) and (5.4) can be adopted to characterize the size of the eddies in the near-wall region for porous media flows, which makes it possible to propose a model for the eddy component of dispersion in this region. Equation (5.2) in the core of the matrix used the Darcy velocity as the characteristic velocity for the mixing length model in the core of the porous matrix. In the near-wall region, it is not possible to use the Darcy velocity as the representative velocity since volume-averaging assumption breaks down as a result of insufficient number of pores required to capture a Representative Elementary Volume. Hence, the local velocity is used instead. Using equations (5.3) and (5.4), the eddy component of dispersion is cast as:

$$\epsilon_M = \kappa y U \qquad 0 < y \leq \frac{\lambda\delta}{\kappa} \tag{5.5}$$

$$\epsilon_M = \lambda\delta U \qquad \frac{\lambda\delta}{\kappa} \leq y \leq \delta \tag{5.6}$$

$$\epsilon_M = 0.02 U_D D_h \qquad y > \delta \tag{5.7}$$

The empirical constants λ and κ have to be adjusted so that the eddy component of dispersion at δ matches the core dispersion value given by equation (5.2). The value of δ is set as one-half of the hydraulic diameter. The justification for this choice is that the near-wall effects seem to be confined to a distance of one-half of the hydraulic diameter away from the wall even when no upstream perturbations

are present (Figure 2.12). Taking this distance as δ would imply that wall damping of eddies are not active beyond $0.5D_h$ and the eddy component of dispersion approaches core value (given by equation (5.2)) for distances greater than one hydraulic diameter from the wall. To ensure that the eddy coefficient of dispersion remains continuous and there are no step changes in its value, the constant λ must be adjusted so that at a distance of δ equal to $0.5D_h$,

$$\lambda \delta U = 0.02 U_D D_h \tag{5.8}$$

From the velocity profiles obtained for unperturbed flow through the porous medium (Figure 2.12), the value of λ is found to vary in the range of 0.018 to 0.04. It must be remembered that the local velocity at a distance of 0.5 D_h away from the wall at different circumferential locations was used to compute λ in equation (5.8). The variations in local velocity when moving circumferentially introduces variation in the value of λ. The coefficient κ is set as 0.41, the same as unobstructed turbulent flow, since there is no constraint that can be imposed on the model to find its value. It might even be arguable that the near-wall region of this flow is similar to the "inner" layer of a turbulent boundary layer and hence this value of κ might be appropriate in the limit that y > 0.

Figure 5 shows the ratio of eddy dispersion to molecular diffusivity in the near wall region obtained using equations (5.5) - (5.7). The value of this ratio in the core is indicated by a horizontal line and is given by equation 5.2. It must be remembered at this point that this plot was generated by extending Prandtl's mixing length theory directly to near-wall flow in the porous medium; not having direct measurements of eddy dispersion prevents one from drawing any further

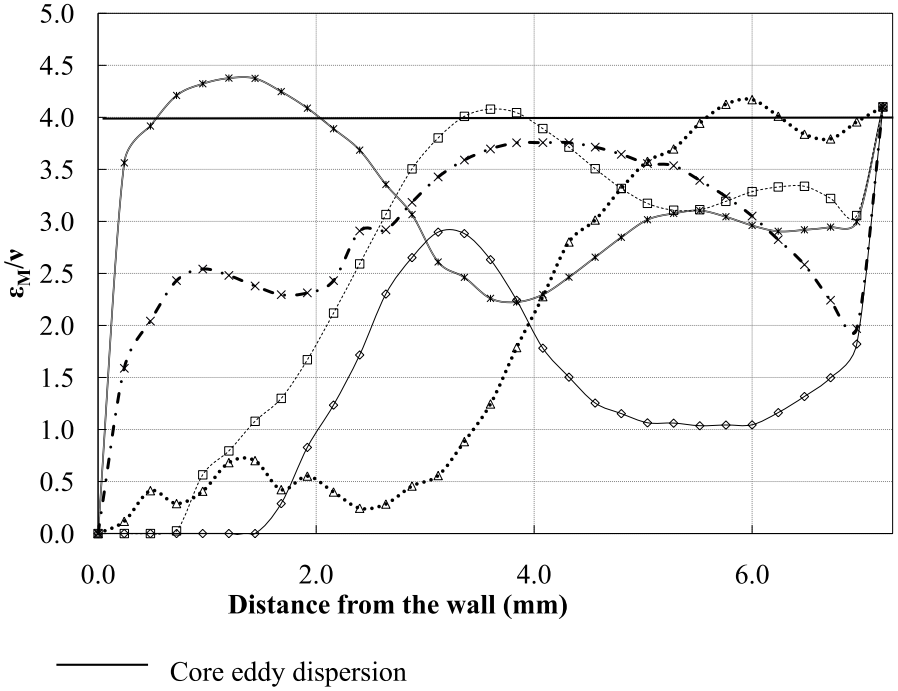

Figure 5.1: Eddy dispersion in the near-wall region obtained by mixing-length hypothesis

conclusion from this figure, and the purpose of this figure is merely to illustrate using the mixing-length hypothesis that eddy dispersion in the near-wall region is smaller than that in the core of the matrix.

The near-wall damping of eddies results in poorer transport characterisitics than in the core of the matrix, preserving upstream disturbances and preventing them from redistributing. Although not attempted here, if the spreading rates of jets and wakes are computed, it might be possible that the spreading rate of near-wall

jets and wakes is much lower than in the core of the matrix.

Chapter 6

Conclusion and Future Work

6.1 Summary of results

The influence of upstream perturbations namely a half-axial jet and a half-axial wake on flow characteristics through a high porosity porous medium were investigated using hotwire anemometry. The radial location of the influences were studied by placing the perturbation near the wall of the test-section and away from the wall in the core of the porous medium.

It was discovered that the disturbances in the near-wall region persist, despite the flow having plenty of opportunity to redistribute as a result of streamwise travel. On the other hand, the disturbances in the core of the porous medium are quickly erased. It was shown by scaling arguments that the redistribution of flow, characterized by eddy-dispersion is weaker in the near-wall region for a distance of atleast half a hydraulic diameter away from the wall. Eddy dispersion is damped

by the viscous wall-boundary layer resulting in poorer transport near the wall. This damping has been attributed as "non-Darcian" effect in the literature and is often coupled with the variation of porosity near the wall. The present study shows that the wall-damping of eddies is not dependent on variation in porosity, and that it would occur even if the porosity were uniform all the way up to the wall.

An extension of Prandtl's mixing length hypothesis was adpoted to characterize wall damping by using the wall-boundary layer thickness as the characteristic length scale of the eddies and the local velocity as the characteristic velocity. For a distance greater than one-half of the hydraulic diameter away from the wall, the eddy dispersion is effective in mixing the core flow. Upstream jets and wakes are erased, and it is suspected that their spreading rates are nearly identical. The velocity profiles obtained for the case with upstream jets and wakes were nearly identical in the core of the matrix.

6.2 Limitations of the present study and future work

One of the limitations of this study is its failure to provide quantitative information on eddy dispersion in different regions of the flow and quantify spreading rates of jets and wakes in the near-wall region of the porous matrix and in its core. Such information would require detailed set of measurements of components of velocity to obtain the eddy dispersion in the near-wall region, and also would require obtaining velocity profiles inside the porous matrix to quantify spreading

rates of jets and wakes. Limited availability of data within the porous medium prevents this study from being any further useful than to show by illustration the transport characteristics in different regions of the flow.

Further extension of the present work should aim to quantify spreading rates of jets and wakes in different regions of the flow. Capturing the effects of eddy-dispersion on spreading rates of jets and wakes would aid modeling and design efforts in applications involving porous media for transport enhancement such as heat exchangers, catalytic converters and thermal storage devices.

References

P. Adnani, I. Catton, and M.A. Abdou. Non-Darcian forced convection in porous media with anisotropic dispersion. *Journal of Heat Transfer*, 117:447, 1995.

A. Amiri and K. Vafai. Analysis of dispersion effects and non-thermal equilibrium, non-darcian, variable porosity incompressible flow through porous media. *International Journal of Heat and Mass Transfer*, 37(6):939 – 954, 1994.

G. S. Beavers and D. D. Joseph. Boundary conditions at a naturally permeable wall. *Journal of Fluid Mechanics*, 30:197–207, 1967.

H.C. Brinkman. A calculation of the viscous force exerted by a flowing fluid on a dense swarm of particles. *Applied Scientific Research*, 1(1):27–34, 1949.

D.F. Van der Merwe and W.H. Gauvin. Velocity and turbulence measurements of air flow through a packed bed. *AIChE Journal*, 17(3):519–528, 1971.

K. Ganesan, T. Simon, and J. Quinnell. Flow through stirling engine regenerators with and without a gap between the matrix and the container wall - part 1: Computation. In *7th International Energy Conversion and Engineering Conference (IECEC), Denver CO*. AIAA, 2009.

M. J. Hall and J. P. Hiatt. Measurements of pore scale flows within and exiting ceramic foams. *Experiments in Fluids*, 20(6):433–440, 04/01/ 1996.

C.T. Hsu and P. Cheng. Thermal dispersion in a porous medium. *International Journal of Heat and Mass Transfer*, 33(8):1587–1597, 1990.

M. L. Hunt and C. L. Tien. Non-darcian convection in cylindrical packed beds. *Journal of Heat Transfer*, 110(2):378–384, 1988.

J.L. Lage, P.S. Krueger, and A. Narasimhan. Protocol for measuring permeability and form coefficient of porous media. *Physics of Fluids*, 17(8):088101, August 2005 2005.

T. Masuoka and Y. Takatsu. Turbulence model for flow through porous media. *International Journal of Heat and Mass Transfer*, 39(13):2803–2809, 9 1996.

T. Masuoka and Y. Takatsu. Turbulence characteristics in porous media. In *Transport Phenomenon in Porous Media Vol. II*. Pergamon, 2002.

G.D. McFadden. Forced thermal dispersion within a representative stirling engine regenerator. Master's thesis, University of Minnesota, 2005.

D.A. Nield. The limitations of the Brinkman-Forchheimer equation in modeling flow in a saturated porous medium and at an interface. *International Journal of Heat and Fluid Flow*, 12(3):269–272, 1991.

Y. Niu. *Fluid Mechanics and Heat Transfer Measurements within a Porous Regenerator under Oscillatory Flow Conditions: Stirling Cycle Thermal Regeneration.* PhD thesis, University of Minnesota, 2005.

J. A. Quinnell. Investigation of the effects of creep on a simulated stirling engine regenerator. Master's thesis, University of Minnesota, Minneapolis, 2008.

P.E. Roach. The generation of nearly isotropic turbulence by means of grids. *International Journal of Heat and Fluid Flow*, 8(2):82 – 92, 1987.

H. Schlichting, K. Gersten, and K. Gersten. *Boundary-layer theory*. Springer Verlag, 2000.

D. Seguin, A. Montillet, J. Comiti, and F. Huet. Experimental characterization of flow regimes in various porous media–II: Transition to turbulent regime. *Chemical Engineering Science*, 53(22):3897–3909, 1998.

S. Taneda. Experimental investigation of the wake behind a sphere at low Reynolds numbers. *J. Phys. Soc. Japan*, 11(10):1104–1108, 1956.

K. Vafai. Convective flow and heat transfer in variable-porosity media. *Journal of Fluid Mechanics*, 147(-1):233–259, 1984.

D.J. Wilson. *An Experimental Investigation of the mean velocity, temperature, and turbulence fields in plane and curved two-dimensional wall jets: Coanda Effect*. PhD thesis, University of Minnesota, 1970.

Appendix A

TSI 1051 Hotwire Anemometer: Operational Caveats

A.1 Description of the TSI 1051 Bridge controls

Velocity profiles were acquired using the TSI 1051 hotwire anemometer bridge. Several hotwire sensors were 'consumed' by this bridge during the early stages of experiments. It must be remembered that this bridge acts as a 1:1 bridge. For instance, if the operating resistance of the sensor, the cable resistance and the probe holder resistance add up to 12 Ω, the control resistor of the anemometer must be set to 12 Ω, and not 60 Ω, as one would, for a 5:1 bridge.

The 1050 series bridge has a failsafe circuit that prevents high current from flowing through the sensor, except when the resistance decade is extremely large. Also, the failsafe circuit will not function if the variable resistance decades are increased

in steps of 10 ohms.

Tables A.1 and A.2 list a brief description of the anemometer bridge controls.

Table A.1: Normal position of the bridge controls for adjusting resistance

Control	Description
RES MEAS	When the RES MEAS control is held down, if the bridge is out of balance, a voltage pulse can be sensed.
RESISTANCE DECADE switches	Measures 0-60 ohms on a 0.01 ohm increment. The value entered in this resistance must be equal to the operating resistance of the probe. For instance, if operating resistance is 11.68 ohms, use the UNITS decade to enter 11 and HUNDREDTHS decade to enter 68.
STANDBY-RUN	When set to STANDBY, it can be used to measure resistance. When set to RUN, current flows through the sensor.

Table A.2: Normal position of the bridge controls for adjusting resistance

Control	Description
REF SET	This is used to adjust the gain of the amplifier. Set this to a value of 15 V when using a hotwire sensor while the STANDBY-RUN control is turned to STANDBY. This must be done after the operating resistance is set. Oscillation control: This control is also used to set the oscillation control when STANDBY-RUN control is in RUN. If oscillations persist even after adjusting STABILITY (see below), turn the REF SET to clockwise. (Remember this has to be done in RUN position) Frequency response: Faster response can be observed when REF SET is set to 20 V in STANDBY.

Continued

Table A.2 – continued from previous page

STABILITY	This control is used to tune the system when the oscillations exist or if the frequency response of the system is poor. Oscillation control: First adjust the TRIM (see below) to minimize oscillations. If that doesn't stop, set the STANDBY-RUN control to RUN, if STABILITY is turned clockwise, some of the oscillations can be eliminated. Frequency response: To maximize frequency response, turn stability control fully clockwise and turn back about 1/4 turn. In general it is not a good idea to mess with STABILITY when adjusting frequency response. Use TRIM and REF SET instead.
	Continued

Table A.2 – continued from previous page

TRIM	Oscillation control: This must be fully counter clockwise if the oscillations exist. Frequency response: To maximize frequency response, turn this clockwise until an oscillation is observed and then turn back slightly.

A.2 Calibration procedure

Unless specified otherwise, the STANDBY-RUN knob should be set to STANDBY.

1. Null out the cable resistance

   (a) Connect the shorting probe to the probe holder and attach the probe holder to the PROBE jack by a BNC cable.

   (b) Set the zero ohm trim pot to the extreme counter-clockwise position (CCW)

   (c) Set about 2 Volts in the display. This is done by holding turning the REF SET clockwise.

   (d) Check to see that the RESISTANCE DECADES are in zero.

   (e) Hold down the RES MEAS switch. The pointer of the analog display will show a value less than 2 V if the decade resistance is smaller than the resistance of the probe cable and the probe holder and a value

greater than 2 V if the decade resistance is larger than that of the cable and the holder.

(f) Adjust the resistance measurement decade knobs (HUNDREDTHS setting) until the pointer reads 2 V again while holding down the RES MEAS switch. Release the RES MEAS switch and press it again. If the pointer shows a deflection, change the RESISTANCE DECADES while holding down the RES MEAS switch. Release the RES MEAS switch and press it down again. If deflection persists, keep repeating this step until no deflection or the smallest amount of deflection is observed. This is the value of the cable and the probe holder resistance.

(g) The value indicated by the HUNDREDTHS decade is the resistance of the cable and the probe holder.

Note: After the resistance has been zeroed out, irrespective of whether the RES MEAS switch is held down or released, the pointer should not deflect. If the pointer deflects, turn the ZERO OHM trim pot further CCW until the pointer does not show any deflection.

2. Set the operating resistance

(a) Now remove the shorting probe and insert the sensor and make sure that the probe resistance is about the same as what is specified by the manufacturers.

(b) The resistance of the probe can be measured by the procedure described above (i.e., keep increasing the RESISTANCE DECADES until the pointer shows no deflection, but be sure to increase the resistance value in small steps, such as 0.5 ohms)

(c) The RESISTANCE DECADES should read a value of about 6 ohms. If the value indicated by the RESISTANCE DECADES is higher, or lower, turn the ZERO OHM trim pot further CCW.

(d) Multiply the number indicated by the RESISTANCE DECADES by a factor of 1.5, add the cable and probe holder resistance and set the RESISTANCE DEACDES to this value. This value must not be higher than the operating resistance of the sensor indicated by the manufacturers.

3. Adjust the frequency response of the bridge

   The STANDBY-RUN position should be in STANDBY and the REF SET should be set to read 2V. (Same positions as above)

   (a) Connect an oscilloscope to the BRIDGE OUTPUT jack of the channel that is being used. Monitor the output to see if there are sine-waves of high frequency in the signal.

   (b) The trim pot TRIM should be in extreme CCW.

   (c) The STABILITY knob should be in the extreme CW position. The oscilloscope output should not show sine-waves now.

   (d) These settings also correspond to the slowest response of the system. If slightly better response is required: Turn the REF SET knob to read 20 V, turn the STABILITY knob about 1/4 turn CCW and the trim pot TRIM should be turned CW until sine-waves begin to appear in the oscilloscope output, and then slightly turned back.

Now the probe is ready to be calibrated. Place the probe in the calibration facility and increase the flow rate through the calibration chamber to record voltage vs.

velocity.

Appendix B

A note on formatting using LaTeX

This thesis was formatted using 80% free software and LaTeX type-setting: LaTeX Editor (LED), a free (as in free-speech, but also as in free-food) and light-weight editor for creating TeX documents and PDFLaTeX, a free and bulky LaTeX compiler that compiles TeX documents into Portable Document Format (PDF) for Windows operating systems. Bibliography was managed using BibTeX and natbib packages. Although the author of this thesis used commercial software for plotting and graphics, the author recommends gnuplot, a free graphics and analysis package that is on par with several professional graphics packages.